PHYSICAL REVIEW D VOLUME 4, NUMBER 11 1 DECEMBER 1971

Weak Production of Nucleon Resonances*

P. A. Zucker
Institute of Theoretical Science, University of Oregon, Eugene, Oregon 97403
(Received 6 July 1971)

We present a dynamical and fully covariant model for the weak production from nucleons of the $N^*(1236)$ and higher-mass resonances. The analytic structure and unitarity of the partial-wave helicity amplitudes are incorporated in this model which has a simple N/D form. Above the $\pi\pi N$ threshold, the excitation and rescattering of hadronic eigenstates are considered. For the excitation mechanism we use pion, nucleon, and vector-meson exchange. By using the conserved vector-current theory and a previous calculation for electroproduction, we ascertain beforehand all the necessary normalizations, which result from the final-state enhancement factors, and thereby perform an absolute calculation for weak production. Predictions are given for the differential and total cross sections in the first four resonance regions, and a favorable comparison is made with the existing data from CERN. Our results for the $N^*(1236)$ are considerably different from the predictions made by Adler in a calculation which treats that one resonance. Since we derive the cross-section formulas keeping all dependence on the lepton mass, we can examine the interesting behavior as the forward direction is approached. The partially conserved axial-vector current hypothesis, its implications for resonance production, and the role of our model in designing a test of it are also discussed.

I. INTRODUCTION

The experimental programs in progress at such centers as Argonne,[1] Brookhaven,[2] and the National Accelerator Laboratory[3] will provide us in the near future with a wealth of new data on inelastic neutrino scattering from nucleons. In anticipation of these results, we now present theoretical predictions for the inelastic processes which result in the formation of an $N^*(1236)$ or a higher-mass resonance. Since our calculation does not include the adjusting of any parameters,[4] it is reasonable to compare the theoretical results with the currently available CERN[5] data on the total cross section for $N^*(1236)$ production. As shown in Sec. V, this agreement is quite good, but more precise experimental values are needed to provide a stringent test of our predictions.

In addition to these experimentally motivated considerations, there are theoretical reasons why a model for the weak production of resonances is interesting and useful. On the one hand, we would like to see if an approach which was quite successful for resonance electroproduction can be extended to axial-vector currents and weak production. On the other hand, we shall see that even the total cross section for weak production provides certain tests of our theory not possible in electroproduction. As a result, models with similar electroproduction predictions can give very different weak predictions. In a different vein, the conserved-vector-current[6] (CVC) theory for inelastic reactions can be studied with the help of such a model. Furthermore, theoretical predictions for resonance production can be useful as input into such other calculations as the quasi-elastic scattering of neutrinos by nuclei. By integrating over the resonance width, we may easily pass to the limit of a narrow resonance viewed as a discrete particle.

A feature of the axial-vector current which has received much attention is its nonconservation. As Adler[7] first pointed out, inelastic neutrino reactions are relevant to this subject since the inelastic cross section for producing a lepton in the forward direction is dominated by the divergence of the axial-vector current (assuming the vector current is conserved). A model like ours is useful in estimating the range in angle or momentum transfer over which the divergence of the axial-vector current dominates the contributions from the other current components. In this work we shall handle the kinematics exactly and analyze the special behavior occuring near the forward direction. Furthermore, we shall examine the PCAC (partially conserved axial-vector current) hypothesis[8,9] for elastic and inelastic processes, and discuss its implications for our model.

In constructing our model, we follow a development similar to one previously completed for electroproduction.[10-12] Actually, this previous calculation does a great deal more for us than just providing an approach already supported by the experimental electroproduction data from SLAC,[13] DESY,[14] CEA,[15] and Stanford.[16] From this previous experience we know the values to use for the ω-

nucleon coupling constant and final-state enhancement factors, enabling us to calculate the weak production without adjusting any parameters. Our previous experience also provides us with some indications on how to handle the pion and vector-meson elastic form factors, the spin-$\frac{1}{2}$ resonances, and a two-channel model. The manner in which our previous work does these things for us will be treated in detail in the text of this article and summarized in this Introduction.

Although there have been other attempts[17,18] to calculate the weak production of the $N^*(1236)$ resonance, we have not seen any other fully relativistic, dynamical calculations which can predict the weak production of the higher-mass resonances. For the particular case of the $N^*(1236)$ resonance, our calculation using partial-wave dispersion relations has much in common with the fixed-momentum-transfer dispersion relations used by Chew, Goldberger, Low, and Nambu,[19] by Fubini, Nambu, and Wataghin[20] (for photoproduction and electroproduction, respectively), and by Adler[18] (for weak production as well). All those calculations are designed for the $N^*(1236)$ and the nonresonant partial waves at lower energies and thereby attempt to avoid the problems posed by inelastic hadronic channels (which we confront in calculating the higher resonances). Since Adler's[18] work is the most thorough and detailed calculation using that approach, we have singled it out for further comparison. Appendix D is devoted to this discussion. Although there are many similarities between our approach and that of Adler,[18] there are several important differences which cause us to give dissimilar predictions for the weak production and for the high-momentum-transfer electroproduction of the $N^*(1236)$. Our numerical predictions are presented in Sec. V. Additional references to earlier works are given in our previous publications.[10-12]

Section II contains the discussion of the kinematics of weak production. If all the final hadronic states are summed over, the cross section given in Sec. II then has the simple form

$$\frac{d^2\sigma}{dW\,dk^2} = \frac{W}{m^2}\frac{G^2}{8\pi}\left(K_1\tilde{W}_1 + K_2\tilde{W}_2 + K_3\tilde{W}_3\right), \tag{1.1}$$

where k^2 is the square of the four-momentum transferred by the leptons to the hadrons, $W=\sqrt{s}$ is the total energy of the final hadronic system in its c.m. frame, m is the nucleon mass, G is the weak coupling constant, and $K_{1,2,3}$ are kinematic factors given below. The $\tilde{W}_{1,2,3}$ are structure functions which describe the hadronic physics, and they are expressed in Sec. II in terms of the helicity amplitudes, which our model is designed to predict. $\tilde{W}_1$ and $\tilde{W}_2$ are analogous to the W_1 and W_2 defined by Drell and Walecka[21] for electroproduction, apart from terms proportional to the lepton mass, m_l.

The kinematic factors are given by

$$\begin{aligned}
K_1 &= 2\frac{k^2+m_l^2}{\epsilon_1^2}, \\
K_2 &= 4\left[1-\frac{k^2+m_l^2}{\epsilon_1 k^2}\left(\frac{k^2+m_l^2}{4\epsilon_1}+k_0^L\right)\right], \\
K_3 &= \frac{k^2}{\epsilon_1 k^*}\frac{m}{W}\left(2-\frac{k^2+m_l^2}{\epsilon_1 k^2}k_0^L\right), \\
k_0^L &= \epsilon_1-\epsilon_2 \\
&= \frac{W^2-m^2+k^2}{2m}, \\
k^{*2} &= k^2+\left(\frac{W^2-m^2-k^2}{2W}\right)^2, \quad k^*>0
\end{aligned} \tag{1.2}$$

where ϵ_1 and ϵ_2 are the initial and final lepton energies measured in the lab frame. k^* corresponds to the three-momentum transferred to the hadrons in their c.m. frame. Since the $\tilde{W}_i$ depend only on W and k^2, Eqs. (1.1) and (1.2) explicitly express the cross section in terms of W, k^2, and ϵ_1.

Our choice to work with the variables W, k^2, and ϵ_1 rather than a set including the lepton lab scattering angle θ, for example, is motivated by several considerations. First we note that our model for the hadronic physics naturally involves W (the resonance mass) and k^2. Then we note that ϵ_1 is an easily measurable quantity while θ is *not* fixed as in electroproduction counter experiments. Furthermore, we are able to express the cross section solely in terms of this set of variables using kinematic quantities $K_{1,2,3}$, which are not complicated (considering that *all* the dependence on the mass of the final lepton has been included). The limit of large ϵ_1 at fixed W and k^2 is quite interesting, and from Eq. (1.2) we see that K_1 and K_3 go to zero while K_2 goes to a constant independent of ϵ_1. As a result, the cross section becomes independent of ϵ_1, leading to regularities (such as a constant total cross section for N^* production) discussed further in Sec. V.

The details of the derivation of the cross section are given in Appendix A; Appendix B summarizes the more general case when a hadron is observed in coincidence with the final lepton. To facilitate comparisons with other notations or with the electroproduction cross section, Sec. II gives the K's in terms of the lepton scattering angle in the lab frame. The analogy with electroproduction is all the more apparent when the parameter ϵ (corresponding to Hand's[22] virtual-photon polarization) given by

$$\epsilon = \left(1+\frac{W^2}{m^2}\frac{2k^{*2}}{k^2}\frac{(1-\beta\cos\theta)^2}{\beta^2\sin^2\theta}\right)^{-1} \tag{1.3}$$

is used. β is the laboratory velocity of the final

lepton, and the fact that $\beta \neq 1$ is important when θ is small.

Throughout this calculation we have kept all the dependence on the lepton mass m_l, and this has not necessitated the use of complicated expressions. All other calculations of which we are aware make approximations regarding the lepton mass. Knowing the dependence on m_l is desirable for a couple of reasons. First, our predictions for $d^2\sigma/dWdk^2$ have large values for $k^2 < 0.1$ GeV^2, and $d\sigma/dk^2$ peaks in this small-k^2 region. For muons, the case of experimental interest, $m_l^2 \approx 0.01$ GeV^2. Second, we are interested in the small-k^2 region because of its bearing on the forward lepton theorem. In Appendix C we investigate this situation more fully, giving a simple derivation of this theorem and showing the approximations (both kinematic and model-dependent) needed. For the purpose of estimating the region in k^2 where the divergence of the axial-vector current dominates, the model-dependent ratio of transverse to longitudinal amplitudes is extremely important. Of course all the "lepton mass corrections" are quite apparent in our treatment and are important for low neutrino energies (greater than 20% for the kinematics of the Argonne experiment, for example).

In order to account for the hadronic physics, we make a model for the partial-wave helicity amplitudes. When speaking generally, we denote these amplitudes by $A(W, k^2)$, suppressing the isospin, spin, parity, and helicity subscripts. A detailed definition of the helicity amplitudes in terms of the matrix elements of the weak hadronic current is given in Sec. II.

For our dynamical model of resonance production, we adopt

$$A(W, k^2) = A^{\text{lhs}}(W, k^2)/D(W) \tag{1.4}$$

and shall summarize the advantages of this choice later on. Here $A^{\text{lhs}}(W, k^2)$ contains the "left-hand singularities" of the amplitude in the complex W plane while $D(W)$ contains the physical cut. Section IV describes our model for A^{lhs} using a set of single-particle-exchange graphs. Section III, on the other hand, discusses the properties along the physical cut and shows how this model incorporates unitarity.

Our basic approach in the discussion of Sec. III is to write a once-subtracted, partial-wave dispersion relation for each amplitude. With the use of unitarity, these dispersion relations become Omnès[23] integral equations:

$$A(W, k^2) = A^{\text{lhs}}(W, k^2) + \frac{W - W_0}{\pi} \int_{W_0}^{\infty} \frac{e^{-i\xi(W')} \sin\xi(W') A(W', k^2)}{(W' - W_0)(W' - W - i\epsilon)}\, dW' . \tag{1.5}$$

Here we have used unitarity to first order in the weak coupling constant, with the result that linear equations emerge. Such an equation has a known[23-25] solution for the amplitude in terms of $A^{\text{lhs}}(W, k^2)$ and the hadronic-scattering phase shift $\xi(W)$. An examination of this solution shows that when there is a sufficiently narrow resonance in the final state, simplifications are possible which result in Eq. (1.4). In this manner Sec. III shows how our model is an approximate solution to the Omnès equation.

From that discussion we also find that the enhancement function $D(W)$ can be expressed in terms of the phase shift $\xi(W)$ by

$$D(W) = \exp\left[-\frac{W - W_0}{\pi} \int_{W_0}^{\infty} \frac{\xi(W')\, dW'}{(W' - W_0)(W' - W - i\epsilon)} \right], \qquad D(W_0) = 1 . \tag{1.6}$$

Unfortunately, the evaluation of this function from the experimental phase shifts is extremely sensitive to the asymptotic behavior assumed for $\xi(W)$.[26] For our present purposes, however, we can avoid a calculation of $D(W)$ and still not introduce any adjustable parameters. First we observe that

$$\int |A(W, k^2)|^2 dW \simeq |A^{\text{lhs}}(W_R, k^2)|^2 \int |D(W)|^{-2} dW \equiv |A^{\text{lhs}}(W_R, k^2)|^2 \mathcal{g} , \tag{1.7}$$

where W_R is the value of W at the resonance peak and $\mathcal{g}$ is seen to be an enhancement factor independent of k^2. Now, as shown in Sec. IV, our model for the vector part of A^{lhs} corresponds to the model for electroproduction so that we satisfy CVC[6] by requiring the value of $\mathcal{g}$ for each resonance to be the same for weak production[27] as for electroproduction. By comparing the electroproduction predictions with the data, we have found phenomenological values for $\mathcal{g}$ which are now used as known inputs for the weak-production calculation.

Although this method for determining $\mathcal{g}$ depends on our model for A^{lhs} (electroproduction), the good agreement of this model with the data out to very large values of k^2 ($k^2 \lesssim 6$ GeV^2) increases our confidence in the resulting value. By way of contrast, the assumptions needed in obtaining $\mathcal{g}$ from the observed phase shifts can yield results easily uncertain by a factor of 4.

Before showing how our model for resonances above the $\pi\pi N$ threshold also reduces to a relation

like Eq. (1.4), let us summarize the desirable features which lead us to take this expression as our model: (i) It has the correct singularity structure since $A^{\rm lhs}(W, k^2)$ has the appropriate left-hand singularities in W, and $D(W)$ has the physical, right-hand cut. (ii) It has built into it the correct threshold dependence on both the weak current and final pion three-momenta (a feature retained by our single-particle-exchange graph model for $A^{\rm lhs}$). (iii) It satisfies the final-state theorem[28] in the region of elastic scattering[29] since, in that region,

$$D(W) = |D(W)|\, e^{-i\xi(W)}. \tag{1.8}$$

(iv) It is an approximate solution to the Omnès equation, provided $A^{\rm lhs}(W, k^2)$ is slowly varying over the resonance. (Nonresonant amplitudes also satisfy Omnès equations which express unitarity, but the solutions are not as simple as the one above.) (v) $D(W)^{-1}$ has a Breit-Wigner shape when $\xi(W)$ passes quickly through $\frac{1}{2}\pi$. (vi) The dependence on k^2 enters entirely through $A^{\rm lhs}(W, k^2)$ and is separated from the term that varies quickly over the resonance. (vii) $A^{\rm lhs}(W, k^2)$ is needed only in the resonance region and not over the entire physical cut. (viii) It corresponds to the simple intuitive picture presented in Fig. 1. First we produce an intermediate state of a given spin and parity, J^π, with an excitation amplitude $A^{\rm lhs}(W, k^2)$. Then, through rescattering, we build up a resonance which subsequently decays. For the $N^*(1236)$ the intermediate state is a pion and a nucleon; but for the higher resonances whose masses are above the $\pi\pi N$ threshold, we shall see below that it is the hadronic eigenstate which rescatters and builds up the resonance.

We note in passing that such a simple picture does not emerge directly from a treatment built in terms of fixed-momentum-transfer dispersion relations. Since the unitarity statement on the physical cut is diagonal with respect to the partial-wave channels, it couples together the various invariant amplitudes for which the fixed-momentum-transfer dispersion relations are written. As a matter of fact, in order to solve this set of coupled dispersion relations in his model, Adler makes simplifying assumptions and then chooses an ansatz based on an analysis of the Omnès equation in the $J^\pi = \frac{3}{2}^+$ partial wave.

For resonances above the $\pi\pi N$ threshold, we can still retain the simplicity of Eqs. (1.4)–(1.6) by viewing each of these resonances as occurring in one hadronic eigenchannel. Such eigenchannels are linear combinations of all the purely hadronic states consistent with the given value of W, and are obtained by diagonalizing the S matrix among these states. Since the unitarity relation is diagonal with respect to the eigenchannels, simple, uncoupled Omnès equations result whose approximate solution is again given by Eq. (1.4). Now, however, $A(W, k^2)$ refers to the amplitude for excitation of the hadronic eigenstate, and $A^{\rm lhs}$ refers to the left-hand singularities in this helicity eigenamplitude. Furthermore, the phase $\xi(W)$ is now the eigenphase shift, which describes scattering wholly within the eigenchannel.[29]

In our previous work on electroproduction, we considered a two-channel model with πN and $\pi N^*(1236)$ as the hadronic channels. As a result, the first eigenamplitude was a linear combination with two terms:

$$A(W, k^2) = a_{\pi N}(W, k^2)\cos\zeta(W) + a_{\pi N^*}(W, k^2)\sin\zeta(W), \tag{1.9}$$

with the mixing angle related to the partial width by

$$\cos^2\zeta(W_R) = \Gamma_{\pi N}/\Gamma. \tag{1.10}$$

After studying the two-channel predictions, we noticed that an interesting and useful simplification was possible. For the noncoincidence electroproduction cross section (where the different helicities are added incoherently), the k^2 dependence given by

$$A^{\rm lhs}(W, k^2) \simeq a^{\rm lhs}_{\pi N}(W, k^2)(\Gamma/\Gamma_{\pi N})^{1/2} \tag{1.11}$$

was very similar to the result using an expression for $A^{\rm lhs}(W, k^2)$ corresponding to Eq. (1.9). For the separate helicity eigenamplitudes, however, such an approximation was not found to produce similar results.

Since the evaluation and partial-wave projection of $a^{\rm lhs}_{\pi N^*}$ is a difficult and intricate matter, the use of Eq. (1.11) presents a considerable simplification. For the purpose of predicting the weak cross sections, we follow this route and save considerable labor on the axial-vector contributions. In Sec. III some electroproduction curves are shown, to indicate how well this approximation works in that calculation. For the $N^*(1236)$ final state, of course, we do not need to make such approximations on $A^{\rm lhs}(W, k^2)$ since only $a^{\rm lhs}_{\pi N}$ contributes.

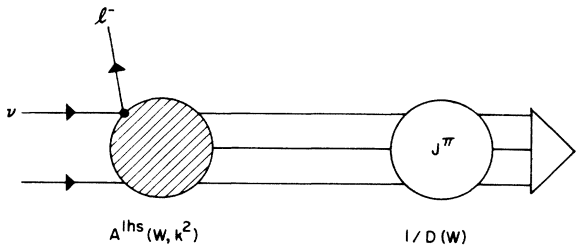

FIG. 1. Model for the weak production of a nucleon resonance showing the excitation of an intermediate hadronic eigenstate which rescatters to build up a resonance of spin and parity J^π and then decays.

Even for this elastic resonance, however, we do need a conceptual framework, such as one built on eigenamplitudes, since the Omnès equation involves an integral over the entire physical cut (W' from W_0 to ∞).

As mentioned previously, Sec. IV contains our discussion of A^{lhs}. Using the preceding approximation, we thus limit ourselves to a discussion of single-particle exchanges contributing to $a^{\text{lhs}}_{\pi N}$. For the vector part of the current, we have chosen nucleon, pion, and vector-meson exchange as our model. By G parity, the ω^0 contributes to the vector current, and the ϕ^0 was found to have small couplings. In electroproduction, the ω-exchange contribution was significant and helped particularly for $k^2 \gtrsim 0.5$ GeV^2. (We treat this meson resonance as though it were a single particle being exchanged.) In addition we discuss the couplings used and elastic form factors present at the weak vertex. When possible, we use the experimental results[30] (such as those of Hofstader and collaborators) for these elastic form factors. Although there are ample data for the nucleon, the pion and vector-meson elastic form factors are hardly known. Faced with this problem, we follow the dictates of simplicity. For the weak vector case we again invoke the conserved-vector-current[6] theory and use the same (isovector) form factors as for electroproduction. In that previous calculation, we gave predictions for the SLAC[13] results. Now that these results are available we can look back and see that pion or vector-meson form factors which asymptotically decrease more slowly than $G_{Ep}(k^2)$ are not consistent with the high-k^2 data within the framework of this model. We therefore continue to make the simple choice and take these elastic form factors proportional to $G_{Ep}(k^2)$.

A similar approach is also followed for the axial-vector part of A^{lhs}. In this case, pion exchange (in the t channel) is ruled out by parity, and ρ exchange replaces ω exchange as a result of G parity. Since the current elastic data[31] suggest a proportionality between the nucleon axial-vector form factor $F_A(k^2)$ and the electromagnetic form factors, we have assumed such a relationship. An additional input required by our inelastic calculation is the induced pseudoscalar form factor $F_P(k^2)$. In the absence of data, we have used the value predicted by PCAC.[8,9] Additionally, we have investigated the extension of PCAC to inelastic processes (resonance production in particular) to see what additional constraints this theory implies for $A^{\text{lhs}}(W, k^2)$.

Our numerical results are presented and discussed in Sec. V. (Some illustrative examples of electroproduction had already been included in Sec. III to show the type of success possible with this approach.) For weak production we predict that the $N^*(1236)$, $N^*(1525)$, $N^*(1688)$, and $N^*(1950)$ are the important levels (like electroproduction), and we present our values for the structure functions $\tilde{W}_{1,2,3}(W, k^2)$ for the excitation of each of these levels. Using these structure functions and the kinematics of Eqs. (1.1) and (1.2), the differential cross section $d^2\sigma/dW dk^2$ can be evaluated at all W, k^2, and ϵ_1. We have additionally integrated over W for each resonance (paying careful attention to the fact that at low ϵ_1 not all the resonance may be in the physical region), and we present the resulting curves for $d\sigma/dk^2$ at some typical values of ϵ_1. The tendency of these curves to approach a universal curve as ϵ_1 increases is quite noticeable, especially for the $N^*(1236)$. As mentioned previously, the region of $k^2 < 0.1$ GeV^2 is of particular interest, and we investigate the various contributions to the cross section in this region. In particular, we examine where and how the k^2 dependence predicted by PCAC can be observed and tested.

By integrating the differential cross section over k^2, we obtain the total cross section as a function of ϵ_1. Although we know from general considerations that such a curve (for a resonance) will rise from threshold and then level off, the height at which the curve becomes flat (in addition to the corresponding value of ϵ_1) is an important prediction of our theory, since we have adjusted no parameters. For the $N^*(1236)$ we compare our prediction (which is noticeably different from Adler's) with the existing data from CERN.[5] Curves are also given for the higher resonances.

In addition to containing a brief summary, Sec. VI discusses the role of CVC and PCAC in our calculation. In regard to more exacting tests of a model for N^* production, we note that coincidence experiments are sensitive to the individual helicity amplitudes.[32,33] Since accurate measurements of the N^* decay distributions at fixed W, k^2, and ϵ_1 seem to be far in the future, we have kept the prediction of $d^2\sigma/dW dk^2$ as our main focus and have made approximations accordingly. It is our hope that the forthcoming data will be accurate enough to provide stringent tests for these noncoincidence predictions presented below.

Appendix D contains a comparison of our approach and results with those of Adler,[18] who calculated $N^*(1236)$ production using a model similar in many ways to ours. Finally, Appendix E gives the expression for $A^{\text{lhs}}(W, k^2)$ resulting from the single-particle exchanges discussed in Sec. IV.

II. PRELIMINARIES

In this section we devote our attention to the general features of weak production which do not require the specific use of a model. Of particular

importance is the definition of the helicity amplitudes, which are used elsewhere in this work. Although our main purpose is to present a discussion containing the particular emphasis appropriate to this calculation, there will be places where the development follows familiar lines. Some ways in which our treatment of the formalism differs from that of others (such as Adler[18]) are that we use partial-wave rather than invariant amplitudes, treat the vector and axial-vector contributions analogously, isolate the divergence of the current in one amplitude independent of all the others, and retain all dependence on the lepton mass. When useful, we will restrict our analysis to the case of a πN final hadronic state. For the noncoincidence cross section, the generalization to any final state is straightforward.

The isobar rest frame (also called the c.m. frame since both the initial and final leptons are represented by an incoming current) is defined by

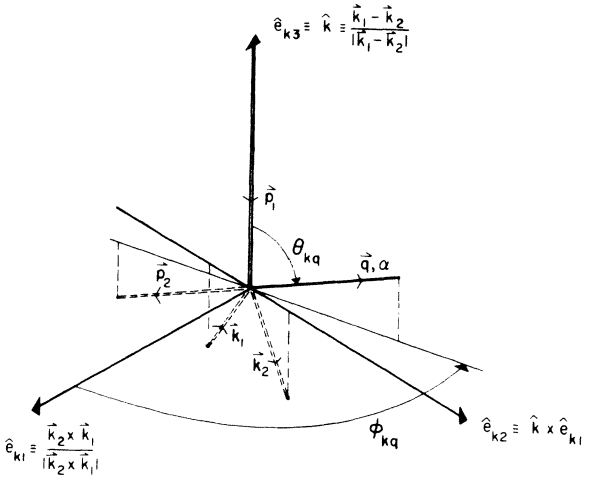

$$\theta_p = \theta_{kq}$$
$$\phi_p = 2\pi - \phi_{kq}$$
$$k_\mu \equiv (k_1 - k_2)_\mu$$
$$k_\mu + p_{1\mu} = q_\mu + p_{2\mu}$$

FIG. 2. Kinematics for the weak production of one pion. The three-momenta and unit vectors are given for the isobar rest frame (also called the c. m. frame since $\vec{k} + \vec{p}_1 = \vec{q} + \vec{p}_2 = \vec{0}$). The initial and final lepton momenta are given by k_1 and k_2, respectively, while p_1 and p_2 refer to the nucleons. For the pion, we label the momentum by q and the (Hermitian) isospin state by α. As defined, k is the momentum transferred by the weak current from the leptons to the hadrons. Also indicated are the pion polar angles θ_{kq} and ϕ_{kq}. The nucleon angles θ_p and ϕ_p are defined to be the angles of $\vec{p}_2$ relative to the triad $(-\hat{e}_{k1}, \hat{e}_{k2}, -\hat{e}_{k3})$ and are easily expressed in terms of the pion angles.

$\vec{p}_1 + \vec{k} = \vec{q} + \vec{p}_2 = \vec{0}$, as shown in Fig. 2. In this frame we write[34] $k_\mu = (\vec{k}^*, ik_0)$ and denote the total hadronic energy by W. By expressing these quantities in an invariant fashion,

$$\begin{aligned} W^2 &= s \\ &= -(p_1 + k)^2 \\ &= -(p_2 + q)^2 , \\ k_0 &= (W^2 - m^2 - k^2)/2W , \\ k^{*2} &= k^2 + k_0^2 , \end{aligned} \tag{2.1}$$

we have extended their definition to all frames as Lorentz scalars. Some other useful definitions and relations follow:

$$\begin{aligned} t &\equiv -(k - q)^2 \\ &= -(p_1 - p_2)^2 \\ &= 2k \cdot q - k^2 + \mu^2 , \\ u &\equiv -(p_1 - q)^2 \\ &= -(p_2 - k)^2 \\ &= 2m^2 - 2k \cdot q - W^2 , \\ P_\nu &\equiv \tfrac{1}{2}(p_1 + p_2)_\nu , \\ 2P \cdot k &= -k \cdot q - W^2 + m^2 , \end{aligned} \tag{2.2}$$

where m is the nucleon mass and μ the pion mass.

For the baryon energies in the c.m. frame, we use E_1 and E_2; the pion has energy ω_q. By θ_p and ϕ_p we denote the baryon angles in this frame:

$$\begin{aligned} \hat{p}_1 &= (0, 0, 1) , \\ \hat{p}_2 &= (\sin\theta_p \cos\phi_p , \sin\theta_p \sin\phi_p , \cos\theta_p) . \end{aligned} \tag{2.3}$$

Sometimes it is convenient to use the pion angles θ_{kq} and ϕ_{kq} which measure the direction of the emerging pion relative to $\hat{k} = -\hat{p}_1$ and are related to the baryon angles by

$$\begin{aligned} \theta_p &= \theta_{kq} , \\ \phi_p &= 2\pi - \phi_{kq} . \end{aligned} \tag{2.4}$$

Our definition is incomplete, however, until the relation to the lepton scattering plane is specified. Figure 2 shows our conventions and defines the unit vectors which will be useful for taking components of the hadronic current.[35] According to these definitions, $\hat{e}_{k1}$ is normal to the lepton scattering plane.[36]

We use the laboratory frame ($\vec{p}_1 = \vec{0}$) to describe the lepton energies and scattering angle, denoted by ϵ_1, ϵ_2, and θ, respectively. The final lepton has velocity β and mass m_l. In order to express the laboratory cross section in terms of W, k^2, and ϵ_1, we need the expressions

$$
\begin{aligned}
k_0^L &= \epsilon_1 - \epsilon_2 \\
&= (W^2 - m^2 + k^2)/2m, \\
|\vec{k}_1 - \vec{k}_2|_{\text{lab}} &= Wk^*/m, \\
k^2 &= (k_1 - k_2)^2 \\
&= 2\epsilon_1\epsilon_2(1 - \beta\cos\theta) - m_l^2 \\
&= 4\epsilon_1\epsilon_2\beta\sin^2(\tfrac{1}{2}\theta) + 2\epsilon_1\epsilon_2(1-\beta) - m_l^2 .
\end{aligned}
\tag{2.5}
$$

The laboratory cross section for producing a πN final state is given (with $L_{\mu\nu}$ and J_μ defined below) by

$$
\frac{d^4\sigma}{dW dk^2 d\Omega_q^*/4\pi} = \frac{W^2}{m^2}\,\frac{q}{4\pi\epsilon_1^2}\,L_{\mu\nu}J_\mu J_\nu^* , \tag{2.6}
$$

where $q \equiv |\vec{q}|$ in the c.m. frame and $d\Omega_q^*$ is the solid angle of the pion, also in the c.m. frame. In reaching this expression, we have used the density of states corresponding to the Jacobian

$$
\left|\frac{\partial\epsilon_2\partial\Omega_2}{\partial W\partial k^2}\right| = \frac{W}{m}\,\frac{\pi}{\epsilon_1\epsilon_2\beta} \tag{2.7}
$$

for fixed ϵ_1 and Ω_q^*. ($d\Omega_2$ is the solid angle in the lab frame for the final lepton.) For the matrix elements of the hadronic current, we have introduced the shorthand notation

$$
J_\mu \equiv \frac{m}{4\pi W}\left(\frac{2\omega_q E_1 E_2 \Omega^3}{m^2}\right)^{1/2}\langle q p_2^{(\text{out})}|J_\mu(0) + J_{\mu 5}(0)|p_1\rangle , \tag{2.8}
$$

$$
J_\mu^* \equiv (\vec{J}^*, iJ_0^*),
$$

and Ω is the normalization volume. The $V-A$ current-current theory of weak interaction gives the form of the lepton vertex, and we have

$$
L_{\mu\nu} = \begin{cases} -\tfrac{1}{2}G^2\,\bar{u}(k_2)\gamma_\mu(1+\gamma_5)u(k_1)\bar{u}(k_1)(1-\gamma_5)\gamma_\nu u(k_2), & \text{incident } \nu \\ -\tfrac{1}{2}G^2\bar{v}(-k_1)(1-\gamma_5)\gamma_\mu v(-k_2)\bar{v}(-k_2)\gamma_\nu(1+\gamma_5)v(-k_1), & \text{incident } \bar{\nu}. \end{cases} \tag{2.9}
$$

For the weak coupling constant G, we use the value obtained from muon decay:

$$
G = 1.023\times 10^{-5}/m^2 . \tag{2.10}
$$

Summing over the lepton spins produces traces which are readily evaluated. The difficulty, however, lies in expressing such dot products as $J\cdot k_1$ and $J\cdot k_2$ in terms of W, k^2, ϵ_1, and the c.m.-frame components of J_μ. In Appendix A this procedure is carried out, and here we summarize the results. For the noncoincidence cross section we obtain

$$
\frac{d^2\sigma}{dW dk^2} = \frac{W}{m^2}\,\frac{G^2}{8\pi}\,(K_1\tilde{W}_1 + K_2\tilde{W}_2 + K_3\tilde{W}_3) . \tag{2.11}
$$

The kinematic factors $K_{1,2,3}$ are given as in Eq. (1.2). For the sake of comparison with other approaches, we repeat these expressions for the K's in terms of W, k^2, and ϵ_1, and also give some equivalent expressions using the laboratory scattering angle θ. Thus we have

$$
\begin{aligned}
K_1 &= 2\,\frac{k^2 + m_l^2}{\epsilon_1^2} \\
&= 4\,\frac{\epsilon_2}{\epsilon_1}\,(1 - \beta\cos\theta), \\
K_2 &= 4\left[1 - \frac{k^2 + m_l^2}{\epsilon_1 k^2}\left(\frac{k^2 + m_l^2}{4\epsilon_1} + k_0^L\right)\right] \\
&= \frac{k^2 + m_l^2}{\epsilon_1^2}\,\frac{k^2 + m_l^2}{k^2}\,\frac{W^2}{m^2}\,\frac{2k^{*2}}{k^2}\,\frac{\epsilon}{1-\epsilon} \\
&= \frac{k^2 + m_l^2}{\epsilon_1^2}\,\frac{k^2 + m_l^2}{k^2}\,\frac{\beta^2\sin^2\theta}{(1-\beta\cos\theta)^2} \\
&= 4\,\frac{\beta^2\epsilon_2^2}{k^2}\sin^2\theta , \\
K_3 &= \frac{k^2}{\epsilon_1 k^*}\,\frac{m}{W}\left(2 - \frac{k^2 + m_l^2}{\epsilon_1 k^2}\,k_0^L\right) \\
&= \frac{k^2 + m_l^2}{\epsilon_1^2}\left(\frac{1+\epsilon}{1-\epsilon}\right)^{1/2} = \frac{k^2}{\epsilon_1^2 k^*}\,\frac{m}{W}\left(\epsilon_1 + \epsilon_2 - \frac{m_l^2}{k^2}\,k_0^L\right),
\end{aligned}
\tag{2.12}
$$

with the parameter ϵ given by Eq. (1.3). From these relations it is apparent that all the K's are positive and that as θ goes to zero, we have ϵ going to zero, K_2 going to zero, K_3 going to half of K_1, and K_1 going to $4(1-\beta)\epsilon_2/\epsilon_1$.

The functions $\tilde{W}_{1,2,3}$, on the other hand, depend on the hadronic physics and are given by

$$\tilde{W}_1(W,k^2)=\tfrac{1}{2}W(4q)\int\frac{d\Omega_q^*}{4\pi}\left(|J^{+1}|^2+|J^{-1}|^2+\frac{m_l^2}{k^{*2}}(|J_C|^2+|J_D|^2)\right),$$

$$\tilde{W}_2(W,k^2)=\frac{m^2}{W}(4q)\int\frac{d\Omega_q^*}{4\pi}\frac{k^2}{2k^{*2}}\left(|J^{+1}|^2+|J^{-1}|^2+\frac{2k^2}{k^{*2}}|J_C|^2\right), \tag{2.13}$$

$$\tilde{W}_3(W,k^2)=W(4q)\int\frac{d\Omega_q^*}{4\pi}\left(\xi|J^{-1}|^2-\xi|J^{+1}|^2+2\frac{m_l^2}{k^{*2}}\,\mathrm{Re}J_C^*J_D\right),$$

with $\xi=+1$ for neutrinos and $\xi=-1$ for antineutrinos. In these expressions a spin sum is understood for the baryons, and other final hadronic states besides πN can be added incoherently. Using the unit vectors given in Fig. 2, we have defined the spherical components of J_μ as

$$J^{\pm1}\equiv\mp\tfrac{1}{2}\sqrt{2}\,(\hat{e}_{k1}\pm i\hat{e}_{k2})\cdot\vec{J}\,. \tag{2.14}$$

In the $\theta=0$ direction we readily see that, of the transverse components, only J^{-1} is present for incident neutrinos and only J^{+1} for antineutrinos, in accordance with angular momentum conservation. For the helicity-zero components of the current, we have defined the following linear combinations:

$$J_C\equiv\frac{k^{*2}}{k^2}\left(J_0-\frac{k_0}{k^*}\vec{J}\cdot\hat{e}_{k3}\right),$$

$$J_D\equiv\frac{k^{*2}}{k^2}\left(\frac{k_0}{k^*}J_0-\vec{J}\cdot\hat{e}_{k3}\right) \tag{2.15}$$

$$=-k^*J\cdot k/k^2.$$

Since $J_D/|\vec{k}|$ is a Lorentz scalar and since $J_C/|\vec{k}|$ is unaffected by Lorentz transformations along $\hat{k}=\hat{e}_{k3}$,[37] these combinations help simplify the kinematical calculations in Appendix A [as well as simplifying the result in Eq. (2.13)]. If the current is conserved, we have the special case

$$J_C=J_0$$

$$=k^*\vec{J}\cdot\hat{e}_{k3}/k_0, \tag{2.16}$$

$$J_D=0.$$

Furthermore, any contribution to J_μ which is proportional to k_μ affects J_D but not J_C. Since k^2 is never equal to zero, these combinations are always finite and linearly independent. In the forward direction, however, k^2 can be quite small, implying that J_C and J_D become quite large. As discussed in Appendix C, it is this kinematical behavior that leads to the forward lepton theorem. From Eq. (2.16) we see contrastingly that for the conserved vector current, J_C does not become kinematically magnified in the forward direction. As a result, the divergence of the axial-vector current dominates. This last point rests, however, on an extrapolation following from

$$\lim_{k^2\to0}k^2J_C=\lim_{k^2\to0}k^2J_D\,. \tag{2.17}$$

Having expressed the cross section in terms of the current components of definite helicity, we now proceed to perform the partial-wave expansions of these components. Following Jacob and Wick,[38,39] we write (always in the c.m. frame)

$$J_\mu e_\mu(\lambda_k)=(4k^*q)^{-1/2}\sum_J(2J+1)\mathfrak{D}^{J*}_{\lambda_1-\lambda_k,\lambda_2}(-\phi_p,-\theta_p,\phi_p)\times\langle\lambda_2|T^J(W,k^2)+U^J(W,k^2)|\lambda_1\lambda_k\rangle\,. \tag{2.18}$$

Here $e_\mu(\lambda_k)$ is a unit vector which projects out $J^{\pm1}$ when $\lambda_k=\pm1$ and J_C or J_D when $\lambda_k=0$.[40] λ_1 and λ_2 are the nucleon helicities, and the meson helicity is zero since we are now considering a πN final state. In this expression, T^J pertains to the vector part of the current and U^J to the axial-vector part.

Since $J_\mu(x)$ and $J_{\mu5}(x)$ have different properties under the parity transformation, it is convenient to introduce states of definite parity. For the initial helicity states we use

$$|\tfrac{3}{2}^\pm\rangle\equiv\tfrac{1}{2}\sqrt{2}\,(|\lambda_1=\tfrac{1}{2},\lambda_k=-1\rangle\mp|-\tfrac{1}{2},1\rangle),$$

$$|\tfrac{1}{2}^\pm\rangle\equiv\tfrac{1}{2}\sqrt{2}\,(|\tfrac{1}{2},1\rangle\mp|-\tfrac{1}{2},-1\rangle), \tag{2.19}$$

$$|L^\pm\rangle\equiv\tfrac{1}{2}\sqrt{2}\,(|\tfrac{1}{2},0\rangle\mp|-\tfrac{1}{2},0\rangle),$$

which have parities $(-1)^{J\pm1/2}$ for the vector current (considered to be like an incident particle with negative intrinsic parity) and the opposite parities for the axial-vector current. For the pion-nucleon final state, the combinations with parities $(-1)^{J\pm1/2}$ are given by

$$\langle\tfrac{1}{2}^\pm|\equiv\tfrac{1}{2}\sqrt{2}\,(\langle\lambda_2=\tfrac{1}{2}|\pm\langle-\tfrac{1}{2}|). \tag{2.20}$$

We now introduce a shorthand notation for the helicity matrix elements involving states of definite parity.[41] Such matrix elements will be re-

ferred to as "helicity amplitudes." For the vector current,

$$
\begin{aligned}
&T^{J^\pi}_{1/2,3/2}(W,k^2)\equiv\langle \tfrac{1}{2}^+|T^J(W,k^2)|\tfrac{3}{2}^+\rangle\,,\\
&T^{J^\pi}_{1/2,1/2}(W,k^2)\equiv\langle \tfrac{1}{2}^+|T^J(W,k^2)|\tfrac{1}{2}^+\rangle\,,\\
&T^{J^\pi}_{1/2,C}(W,k^2)\equiv\langle \tfrac{1}{2}^+|T^J(W,k^2)|L^+,\text{“}C\text{”}\rangle\,,\\
&T^{J^\pi}_{1/2,D}(W,k^2)\equiv\langle \tfrac{1}{2}^+|T^J(W,k^2)|L^+,\text{“}D\text{”}\rangle\,,
\end{aligned}
\tag{2.21}
$$

where the "C" and "D" combinations are defined in Eqs. (2.15) and (2.18). For the axial-vector current, we have corresponding relations such as

$$
U^{J^\pi}_{1/2,3/2}(W,k^2)\equiv\langle \tfrac{1}{2}^+|U^J(W,k^2)|\tfrac{3}{2}^-\rangle\,. \tag{2.22}
$$

In all cases the final state has parity $(-1)^{J\pm 1/2}$. When convenient, we shall use the alternate notation $l\pm$ for J^π, where l is defined to be $J\mp\frac{1}{2}$ and is the orbital angular momentum of the pion. The signs in $l\pm$ always correspond to those of the *final* helicity state. When referring to the helicity amplitudes collectively, we will drop the subscripts and use the notation $A(W,k^2)$.

For simplicity and convenience we have chosen to work with helicity matrix elements rather than multipole moments. The various phase conventions contained in our definition of the helicity amplitudes are most easily summarized by giving the relation to the traditional multipoles for single-pion production used by Chew, Goldberger, Low, and Nambu[19] and others. In this comparison the helicity amplitudes describe an electromagnetic current. Section IV contains a discussion of how the weak vector case is related to the electromagnetic by CVC. We have (apart from a factor of the charge on the proton)

$$
\begin{aligned}
&(4k^*q)^{1/2}(l+1)M_{l+}=-\tfrac{1}{2}i\sqrt{2}\left[T^{l+}_{1/2,1/2}-\left(\frac{l+2}{l}\right)^{1/2}T^{l+}_{1/2,3/2}\right],\\
&(4k^*q)^{1/2}(l+1)E_{l+}=-\tfrac{1}{2}i\sqrt{2}\left[T^{l+}_{1/2,1/2}+\left(\frac{l}{l+2}\right)^{1/2}T^{l+}_{1/2,3/2}\right],\\
&(4k^*q)^{1/2}lM_{l-}=-\tfrac{1}{2}i\sqrt{2}\left[T^{l-}_{1/2,1/2}-\left(\frac{l-1}{l+1}\right)^{1/2}T^{l-}_{1/2,3/2}\right],\\
&(4k^*q)^{1/2}lE_{l-}=+\tfrac{1}{2}i\sqrt{2}\left[T^{l-}_{1/2,1/2}+\left(\frac{l+1}{l-1}\right)^{1/2}T^{l-}_{1/2,3/2}\right],\\
&(4k^*q)^{1/2}C_{l\pm}=iT^{l\pm}_{1/2,C}\,.
\end{aligned}
\tag{2.23}
$$

Using the preceding definitions, we can insert the partial-wave expansion into Eq. (2.13), integrate over angles, sum over spins, and obtain

$$
\begin{aligned}
\tilde{W}_1(W,k^2)&=\tfrac{1}{2}W\sum_{J^\pi}\frac{J+\frac{1}{2}}{k^*}\Big[|T^{J^\pi}_{1/2,3/2}|^2+|T^{J^\pi}_{1/2,1/2}|^2+|U^{J^\pi}_{1/2,3/2}|^2+|U^{J^\pi}_{1/2,1/2}|^2\\
&\qquad+\frac{m_l^2}{k^{*2}}\left(|T^{J^\pi}_{1/2,C}|^2+|U^{J^\pi}_{1/2,C}|^2+|U^{J^\pi}_{1/2,D}|^2\right)\Big],\\
\tilde{W}_2(W,k^2)&=\frac{m^2}{W}\sum_{J^\pi}\frac{J+\frac{1}{2}}{k^*}\frac{k^2}{2k^{*2}}\left[|T^{J^\pi}_{1/2,3/2}|^2+|T^{J^\pi}_{1/2,1/2}|^2+|U^{J^\pi}_{1/2,3/2}|^2+|U^{J^\pi}_{1/2,1/2}|^2+2\frac{k^2}{k^{*2}}\left(|T^{J^\pi}_{1/2,C}|^2+|U^{J^\pi}_{1/2,C}|^2\right)\right],\\
\tilde{W}_3(W,k^2)&=W\sum_{J^\pi}\frac{J+\frac{1}{2}}{k^*}\left(2\xi\,\mathrm{Re}\,T^{J^\pi *}_{1/2,3/2}U^{J^\pi}_{1/2,3/2}-2\xi\,\mathrm{Re}\,T^{J^\pi *}_{1/2,1/2}U^{J^\pi}_{1/2,1/2}+2\frac{m_l^2}{k^{*2}}\,\mathrm{Re}\,U^{J^\pi *}_{1/2,C}U^{J^\pi}_{1/2,D}\right).
\end{aligned}
\tag{2.24}
$$

Again, $\xi=+1$ for neutrinos and -1 for antineutrinos. For these relations we have taken the vector current to be conserved:

$$
T^{J^\pi}_{1/2,D}(W,k^2)=0\,. \tag{2.25}
$$

It is now clear that $\tilde{W}_3$ contains the vector–axial-vector interference, while $\tilde{W}_1$ and $\tilde{W}_2$ are closely related to the Drell and Walecka[21] structure functions W_1 and W_2. (For the partial-wave expansion of W_1 and W_2 in electroproduction, see Appendix A of Ref. 33.) In general, the tensor

$$
W_{\mu\nu}=4qW\sum_{\text{spins}}\int\frac{d\Omega_q^*}{4\pi}J_\mu J_\nu^* \tag{2.26}
$$

can be expanded in terms of six independent structure functions, three of which are needed only if the current is not conserved. Our $\tilde{W}_{1,2,3}$ are then the three combinations of these six structure functions which are present after contraction with the lepton tensor $L_{\mu\nu}$.

Appendix B contains the expression for the cross section if the pion angles are not integrated over. Cross sections for polarized baryons can also be derived using the same procedure and kinematics, but are not given here.

The isospin properties of the helicity amplitudes are easily summarized. As in Fig. 2, we denote the Hermitian isospin state of the final pion by α. Taken between two nucleon isospinors, each helicity amplitude ($T^{J\pi}$ and $U^{J\pi}$ denoted by A) has the general structure

$$A(W,k^2)=\tfrac{1}{2}(\tau_\alpha\tau_+ + \tau_+\tau_\alpha)A^{(+)}(W,k^2) + \tfrac{1}{2}[\tau_\alpha,\tau_+]A^{(-)}(W,k^2) \tag{2.27}$$

for incident neutrinos. For incident antineutrinos, the $A^{(+)}$ and $A^{(-)}$ are unaffected, and τ_+ is replaced by τ_-. Forming final states of definite isospin then leads to

$$\begin{aligned}
&A(\tfrac{3}{2},\nu p)=-\tfrac{1}{2}\sqrt{2}\,(A^{(+)}-A^{(-)}),\\
&A(\tfrac{3}{2},\nu n)=-\tfrac{1}{6}\sqrt{6}\,(A^{(+)}-A^{(-)}),\\
&A(\tfrac{1}{2},\nu n)=-\tfrac{1}{3}\sqrt{3}\,(A^{(+)}+2A^{(-)}),\\
&A(\tfrac{1}{2},\nu p)=0=A(\tfrac{1}{2},\bar\nu n),\\
&A(\tfrac{1}{2},\bar\nu p)=-\tfrac{1}{3}\sqrt{3}\,(A^{(+)}+2A^{(-)}),\\
&A(\tfrac{3}{2},\bar\nu n)=+\tfrac{1}{2}\sqrt{2}\,(A^{(+)}-A^{(-)}),\\
&A(\tfrac{3}{2},\bar\nu p)=+\tfrac{1}{6}\sqrt{6}\,(A^{(+)}-A^{(-)}),
\end{aligned} \tag{2.28}$$

where we have indicated in parentheses the final isospin and the initial particles. For isospin-$\frac{3}{2}$ final states, the difference between proton and neutron targets is only a factor $\sqrt{3}$, while in the isospin-$\frac{1}{2}$ case, only one possibility is permitted. The $\bar\nu p$ and $\bar\nu n$ are the same as the νn and νp amplitudes, respectively, except for a sign in the isospin-$\frac{3}{2}$ case. All our results will be given for final states of definite isospin.

III. DYNAMICAL MODEL

In this section we further analyze the dynamical model given in Eq. (1.4). Having already enumerated in the Introduction the many desirable features that lead us to choose $A^{\rm lhs}/D$ as our model for the resonant helicity amplitudes, we now focus our attention on those features pertaining to unitarity and the Omnès equation. In particular, we examine the exact Omnès solution and discuss the approximations that result in $A^{\rm lhs}/D$. Since this treatment is identical to the corresponding discussion for electroproduction (the differences enter in the models for $A^{\rm lhs}$, which are discussed in Sec. IV), we refer the reader to Ref. 12 for a more detailed discussion. Finally, we evaluate the model by reviewing some of the electroproduction predictions and data.

For each helicity amplitude $a(W,k^2)$, we write a partial-wave dispersion relation,

$$a(W,k^2)=a^{\rm lhs}(W,k^2)+\frac{W-W_0}{\pi}\int_{W_0}^{\infty}\frac{{\rm Im}a(W',k^2)dW'}{(W'-W_0)(W'-W-i\epsilon)}, \tag{3.1}$$

explicitly displaying the physical cut. The singularities located elsewhere are contained in $a^{\rm lhs}$. Since we wish to include the possibility that ${\rm Im}a(W',k^2)$ does not go to zero at large W', we have chosen to subtract the dispersion relation. By using the fact that

$$a(W_0,k^2)=a^{\rm lhs}(W_0,k^2)=0 \tag{3.2}$$

in every partial wave, we know we have a zero subtraction constant. If additional subtractions are made, the solution is similarly obtained, but there will be additional subtraction constants to ascertain.

In order to evaluate the imaginary part along the cut, we use unitarity. From Jacob and Wick,[38] we know that the unitarity relation for helicity amplitudes does not combine different angular momenta. (In contrast, fixed-t dispersion relations suffer from the fact that unitarity relates the imaginary part of one invariant amplitude to the other invariant amplitudes.) Since the weak coupling constant is quite small, we may neglect terms in the unitarity relation containing the product of two weak helicity amplitudes. As a result, the unitarity relation will be linear in the helicity amplitudes and therefore will not relate amplitudes of differing initial helicity. On the other hand, unitarity generally does relate the amplitudes with different final helicity states, since above the $\pi\pi N$ threshold there is more than one hadronic channel present.

In order to solve this problem and obtain uncoupled Omnès equations, we consider the S matrix for a given partial wave. It will have a row and a column for each hadronic channel and also for each helicity corresponding to the weak current plus a nucleon. Of particular interest to us here are the entries for a weak-plus-nucleon initial state and hadronic final state, but these elements are related to the purely hadronic matrix elements by the unitarity constraint. Since the hadronic part of this S matrix is symmetric (assuming time-reversal invariance for the strong interactions) and unitary by itself (neglecting terms proportional to the square of the weak coupling constant), it can be diagonalized by a real, orthogonal transformation. If $|e_i\rangle$ is a hadronic eigenstate defined by this transformation, we then have

$$\langle e_j|S^{J\pi}(W)|e_i\rangle=\delta_{ij}\exp[2i\xi_j^{J\pi}(W)]. \tag{3.3}$$

The eigenphase shift $\xi_j(W)$ defined by this relation

is a real function for all W because the eigenvalues of a unitary matrix have unit magnitude.

Once the hadronic part of the S matrix is in diagonal form, the unitarity relation is quite simple. For the amplitudes corresponding to an initial weak-current-plus-nucleon state and a final hadronic eigenstate [called "helicity eigenamplitudes" and denoted by $A(W, k^2)$], we have

$$\mathrm{Im}A(W, k^2) = e^{-i\xi(W)} \sin\xi(W)\, A(W, k^2)\,. \tag{3.4}$$

Since it is the helicity eigenamplitudes which satisfy a simple unitarity relation, we choose to write dispersion relations for these quantities rather than for the usual helicity amplitudes. Thus, we write relations as in Eq. (3.1) for each helicity eigenamplitude, $A(W, k^2)$. By inserting the unitarity relation of Eq. (3.4), we obtain

$$A(W, k^2) = A^{\mathrm{lhs}}(W, k^2) + \frac{W - W_0}{\pi} \int_{W_0}^{\infty} \frac{e^{-i\xi(W')} \sin\xi(W')\, A(W', k^2)\, dW'}{(W' - W_0)(W' - W - i\epsilon)} \tag{3.5}$$

for each helicity eigenamplitude. Since the unitarity relation does not relate different eigenamplitudes, these integral equations are uncoupled. Since the unitarity relation is linear in the eigenamplitude, these integral equations are linear and can be solved for $A(W, k^2)$ in terms of $A^{\mathrm{lhs}}(W, k^2)$ and $\xi(W)$.

Although we have obtained such a tractable system of equations, we have made very few approximations or assumptions. In particular, we assumed that second-order terms in the weak coupling constant could be neglected and that the helicity eigenamplitudes satisfy once-subtracted dispersion relations. Furthermore, time-reversal invariance of the strong interactions implies that the transformation from the physical states to the hadronic eigenstates is real and orthogonal. Subsequently, we shall make approximations for A^{lhs} and ξ, but first we present the exact mathematical solution to Eq. (3.5).

The solution for the unsubtracted form of Eq. (3.5) has been given by Omnès[23] and independently by Muskhelishvili.[24] The latter also includes a thorough mathematical discussion of the procedure, making the extension to the subtracted case (discussed in Ref. 12) relatively simple. With the subtraction, the exact[42] mathematical solution becomes

$$A(W, k^2) = A^{\mathrm{lhs}}(W, k^2) + X(W)\, \frac{W - W_0}{\pi} \int_{W_0}^{\infty} \frac{\sin\xi(W') A^{\mathrm{lhs}}(W', k^2)\, dW'}{|X(W')|\,(W' - W_0)(W' - W - i\epsilon)}\,,$$
$$X(W) \equiv \exp\left[\frac{W - W_0}{\pi} \int_{W_0}^{\infty} \frac{\xi(W')\, dW'}{(W' - W_0)(W' - W - i\epsilon)}\right]. \tag{3.6}$$

By adding and subtracting $A^{\mathrm{lhs}}(W, k^2)$ under the integral and by using the properties of the Cauchy representation of $[(z - W_0)X(z)]^{-1}$ in the complex z plane, we obtain[12] an alternate form[43] of the solution:

$$A(W, k^2) = X(W)\left[A^{\mathrm{lhs}}(W, k^2) + \frac{W - W_0}{\pi} \int_{W_0}^{\infty} \frac{\sin\xi(W')[A^{\mathrm{lhs}}(W', k^2) - A^{\mathrm{lhs}}(W, k^2)]}{|X(W')|\,(W' - W_0)(W' - W)}\, dW'\right]. \tag{3.7}$$

In this form several important properties are apparent. First we notice that the integral in this relation has zero discontinuity across the physical cut, since the numerator is zero when $W = W'$. As a result, this integral is real, and therefore

$$\frac{A(W, k^2)}{|A(W, k^2)|} = \frac{X(W)}{|X(W)|} = e^{i\xi(W)}\,, \tag{3.8}$$

showing that the amplitude obeys a final-state theorem for all physical W. Second, we note that this solution has a general N/D form, since the bracket in Eq. (3.7) has singularities only for complex W away from the physical region (the N function) and since $X(W)^{-1}$ has the physical cut (the D function).

Although the expression in Eq. (3.7) is mathematically exact and satisfies unitarity, it is extremely difficult to evaluate. On the one hand, there is a complicated integral requiring values for A^{lhs} at all $W' > W_0$, and, on the other hand, our knowledge of $A^{\mathrm{lhs}}(W, k^2)$ and $\xi(W)$ is limited. When a resonance is present in the eigenamplitude, however, we can make some approximations to simplify the solution in Eq. (3.7).

At this point, we should emphasize that our goal is not to derive a particular model. Rather, we have already assumed the A^{lhs}/D model given in Eq. (1.4) for the reasons indicated in the Introduction. Among those reasons was the statement that, for a resonance, A^{lhs}/D is an approximate solution to the Omnès equation. Now it is our aim to show what approximations are needed to obtain an A^{lhs}/D result from the Omnès solution in Eq. (3.7). Although we present these approximations with some arguments supporting their reasonability, the real justification of a model must come from its com-

parison with the data. Fortunately, there are plentiful data on resonance electroproduction, and such a comparison for a similar model has already been performed.[11,12] Below we shall review some results from electroproduction to get an indication of how well such a model can be expected to work. The good agreement out to large values of k^2 is particularly encouraging since approximations in $A^{\rm lhs}$, as well as the assumption of the $A^{\rm lhs}/D$ model, are being tested.

From an examination of Eq. (3.7), we see that the $A^{\rm lhs}/D$ model results if we can neglect the integral relative to $A^{\rm lhs}$,

$$\frac{W-W_0}{\pi}\int_{W_0}^{\infty}\frac{\sin\xi(W')}{|X(W')|}\,\frac{A^{\rm lhs}(W',k^2)-A^{\rm lhs}(W,k^2)}{(W'-W_0)(W'-W)}\,dW' \ll A^{\rm lhs}(W,k^2)\,, \tag{3.9}$$

when W is near W_R. Let us first analyze the function $F(W')$ given by

$$F(W')\equiv\frac{1}{\pi}\frac{W_R-W_0}{W'-W_0}\,\frac{\sin\xi(W')}{|X(W')|}\,. \tag{3.10}$$

The eigenphase ξ starts from zero at threshold, goes rapidly through $\frac{1}{2}\pi$ at resonance, and then, depending on one's model, may go asymptotically to π or may decrease to some other limit.[44] As a result, $\sin\xi$ peaks in the region of the resonance. On the other hand, $|X(W')|^{-1}$ possesses a dip there so that the product, $\sin\xi(W')|X(W')|^{-1}$, remains roughly constant. An expansion for W' about the resonance value W_R helps support this assertion:

$$\begin{aligned}X(W)&\equiv\frac{1}{D(W)}\\&\cong\frac{1}{\mathrm{Re}'D(W_R)(W-W_R)+i\,\mathrm{Im}D(W_R)}\\&=\frac{1}{\mathrm{Re}'D(W_R)}\,\frac{1}{W-W_R+\frac{1}{2}i\Gamma}\,,\end{aligned} \tag{3.11}$$

$$\mathrm{Re}'D(W_R)\equiv\left[\frac{d}{dW}\,\mathrm{Re}D(W)\right]_{W=W_R}\,,$$

$$\Gamma\equiv 2\,\mathrm{Im}D(W_R)/\mathrm{Re}'D(W_R)\,.$$

Since the Breit-Wigner shape thus obtained is a reasonable representation for a resonance (and agrees nicely with the electroproduction data[45]), we infer that $\mathrm{Im}D(W)$ varies only slightly from its resonance value. As a result, we have

$$\begin{aligned}-\mathrm{Im}D(W)&=-\mathrm{Im}[\,|D(W)|e^{-i\xi}]\\&=\sin\xi(W)|D(W)|\\&\cong-\mathrm{Im}D(W_R)=|D(W_R)|\,,\end{aligned} \tag{3.12}$$

showing indeed that $\sin\xi(W)|D(W)|$ is approximately constant. In electroproduction we saw that $|D(W_R)|$ was typically in the vicinity of 0.2 for the prominent resonances.

If the eigenphase shift approaches π asymptotically, then $\sin\xi(W)|D(W)|$ remains small in the high-energy tail of the resonance. If, on the other hand, $\xi(W)$ reaches a maximum less than π and decreases to a nonzero asymptotic value, $\sin\xi$ does not go to zero, and the behavior in the tail will be different. In Refs. 11 and 46, models for the eigenphase shifts are developed which have this latter behavior. Although $|X(W)|^{-1}$ then grows large asymptotically, the subtracted form of the Omnès equation[47] guarantees the presence of a $(W-W_0)^{-1}$ factor which suppresses this growth. Using such a model[11] for ξ as an example, we find that the factor $F(W)$ given in Eq. (3.10) has a value of about $0.2/\pi$ in the resonance region, grows in the tail to about $0.6/\pi$ near $W+2\Gamma$, and then decreases monotonically to zero. Although this numerical estimate is based on a particular model for $\xi(W)$, it does support the assertion that while $F(W)$ may grow in the tail region, it does not become large.[48]

The remaining factor in the integrand of Eq. (3.9) gives the variation of $A^{\rm lhs}$ over the region of integration. Since $A^{\rm lhs}$ does not have singularities near the physical cut, we expect that it will vary slowly in the physical region.[49] In particular, the variation across the resonance is approximated as slight. For W near W_R we take

$$\frac{A^{\rm lhs}(W,k^2)-A^{\rm lhs}(W_R,k^2)}{W-W_R}\simeq\left[\frac{d}{dW}A^{\rm lhs}\,(W,k^2)\right]_{W=W_R} \ll A^{\rm lhs}(W,k^2)/\Gamma\,. \tag{3.13}$$

When W is not near W_R, the $(W-W_R)^{-1}$ factor is small and will dominate the growth of $A^{\rm lhs}(W,k^2)-A^{\rm lhs}(W_R,k^2)$.[50] When integrating over dW, the decreasing function $F(W)$ is also present in the integrand, with the result that the asymptotic region gives a small contribution to the total value of the integral. Combining all these observations and approximations about the integral in Eq. (3.9), we estimate that it is indeed much smaller than $A^{\rm lhs}(W,k^2)$ when W is near W_R. In Eq. (3.7) we then neglect the integral and obtain the approximate Omnès solution for a resonance:

$$\begin{aligned}A(W,k^2)&\simeq X(W)A^{\rm lhs}(W,k^2)\\&=A^{\rm lhs}(W,k^2)/D(W)\,.\end{aligned} \tag{3.14}$$

Of the many advantages possessed by this approximate Omnès solution, we emphasize its simplicity, the separation of the k^2 dependence from the hadronic physics, and the necessity of knowing $A^{\rm lhs}(W,k^2)$ *only* in the region of the resonance. In the Introduction we listed these and other reasons

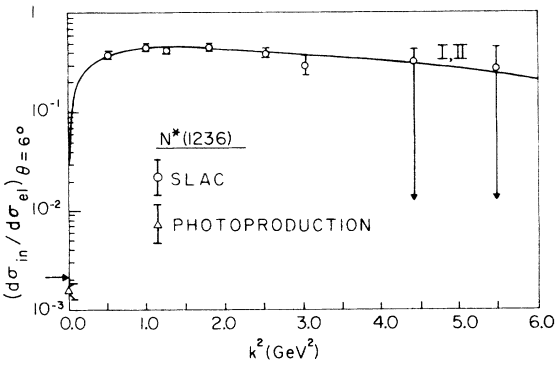

FIG. 3. Comparison for the $N^*(1236)$ of the electroproduction predictions from Ref. 12 with the most recent 6° data from SLAC (Ref. 51). For the photoproduction point the analysis of Ref. 52 was used. The ratio of inelastic to elastic cross sections used as the ordinate is given in Eq. (3.15). The arrow indicates the prediction when $k^2=0$.

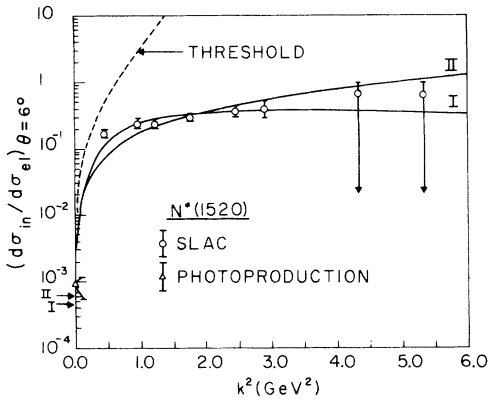

FIG. 4. Same as Fig. 3 but now for the $N^*(1520)$ region. region. In addition, the pure threshold behavior [given in Eq. (5.33) of Ref. 11] is indicated. The curves labeled I and II are explained in the text.

why Eq. (3.14) is desirable as a model for the helicity eigenamplitudes. Now, we have seen what assumptions and approximations are required to obtain it from the solution of the Omnès equation.

In order to exhibit some of the consequences of the $A^{\rm lhs}/D$ model and to see some of its strengths and weaknesses, we now present some results for electroproduction taken from Ref. 12. Figures 3 and 4 contain the comparison of the model and the most recent SLAC data[51,52] for the $N^*(1236)$ and $N^*(1520)$ resonance regions. Although comparisons have also been made for the $N^*(1688)$ and $N^*(1950)$ regions, their results and implications are very similar to those for the $N^*(1520)$, and we therefore do not give the curves for these two levels here.

On the ordinate is plotted the ratio of the resonance cross section (at fixed incident electron energy and angle) to the elastic cross section evaluated at the same ϵ_1, θ, and k^2. After cancellation of some kinematic factors, we have

$$\frac{d\sigma_{\rm in}}{d\sigma_{\rm el}}=\frac{(d\sigma/d\Omega)_{\rm Res}}{(d\sigma/d\Omega)_{\rm el}}$$
$$=\frac{(W_R/m)\int dW[2W_1(W,k^2)_{\rm Res}\tan^2(\frac{1}{2}\theta)+W_2(W,k^2)_{\rm Res}]}{(k^2/2m^2)G_{Mp}^{\ 2}(k^2)\tan^2(\frac{1}{2}\theta)+\{[G_{Ep}^{\ 2}(k^2)+(k^2/4m^2)G_{Mp}^{\ 2}(k^2)]/(1+k^2/4m^2)\}}. \quad (3.15)$$

The W_1 and W_2 occurring above are the structure factors introduced by Drell and Walecka,[21] while G_{Mp} and G_{Ep} are the elastic form factors of the proton. In Sec. IV we see how scaling relations are used in our model for $A^{\rm lhs}$, with the result that we calculate the ratio $A^{\rm lhs}/G_{Ep}$ directly. Since the proton form factors obey a scaling relation, the ratio in Eq. (3.15) depends on $A^{\rm lhs}/G_{Ep}$ and is therefore predicted by the electroproduction model without any assumptions about $G_{Ep}(k^2)$. For the data, the experimental $G_{Ep}(k^2)$ and $G_{Mp}(k^2)$ were used in finding this ratio. In contrast to the case of electroproduction, we choose to plot $d\sigma/dk^2$ rather than a corresponding ratio for the weak predictions in Sec. V. The reason for this is that we also present our predictions integrated over k^2. At that point, values for $G_{Ep}(k^2)$ must be introduced in order to perform the integration.

In the calculation of the electroproduction predictions given in Figs. 3 and 4, we have again approximated $A^{\rm lhs}$ to be slowly varying across the resonance:

$$\int |A(W,k^2)|^2 dW \simeq |A^{\rm lhs}(W_R,k^2)|^2 \int |D(W)|^{-2} dW$$
$$\equiv |A^{\rm lhs}(W_R,k^2)|^2 \mathcal{I}. \quad (3.16)$$

Furthermore, we have assumed that each resonance occurs in only one hadronic eigenchannel. Although $\mathcal{I}$ can be determined, in principle, from the eigenphase shift, using Eq. (3.6), such a determination is quite sensitive to assumptions about the asymptotic behavior of the eigenphase shift (as discussed further in Sec. I and Appendix D). As a result, we have chosen to determine $\mathcal{I}$ empirically for each resonance. Thus the curves in Figs. 3 and 4 are

normalized to the data. Having determined these enhancement factors from electroproduction, we use them as known inputs for our weak calculation. As a result, our weak calculation does not have any parameters to be adjusted. Furthermore, for the purposes of giving the area under a resonance, Eq. (3.16) shows that knowledge of ϑ is sufficient information regarding the hadronic physics—all other consequences of the eigenphase shift can be ignored.

In the comparison for the $N^*(1236)$ given in Fig. 3, we see that the electroproduction predictions agree very well with the SLAC data out to large values of k^2. Although there is some discrepancy at photoproduction (the arrow indicates where the curve starts), the abrupt rise and leveling off are confirmed by the data. Even though the sharpness of this rise depends to some extent on the kinematics (being most pronounced at small values of θ), the region of leveling and subsequent flatness out to large k^2 are important, model-dependent results.[53] By way of contrast, Adler's[18] calculation gives predictions that fall below the data for $k^2 \gtrsim 0.5$ GeV^2.

For the $N^*(1520)$ displayed in Fig. 4, we again note the sharp rise followed by an abrupt leveling. A threshold calculation[11] (based on the kinematics for small three-momentum of the virtual photon in the c.m. frame) is included for comparison and is normalized to photoproduction. Since the threshold curve does not level off, we see that the location at which and the abruptness with which our curves turn over are not related to a special kinematic limit. (When $k^2 = 0$, the three-momentum of the virtual photon is already large.)

The curves labeled I and II refer to two different calculations. For the eigenamplitude, a two-channel calculation[11,12] was performed using πN and $\pi N^*(1236)$ as the hadronic final states. In terms of the physical channels, the excitation function is given by

$$A^{\rm lhs}(W, k^2) \simeq a^{\rm lhs}_{\pi N}(W, k^2)\cos\zeta(W_R) + a^{\rm lhs}_{\pi N^*}(W, k^2)\sin\zeta(W_R)\,, \qquad (3.17)$$

$$\cos^2\zeta(W_R) = \Gamma_{\pi N}/\Gamma\,,$$

and we refer to this as model II. A particularly interesting result learned from our experience with electroproduction and displayed in Fig. 4 is that a much simpler model,

$$A^{\rm lhs}(W, k^2) \simeq a^{\rm lhs}_{\pi N}(W, k^2)(\Gamma/\Gamma_{\pi N})^{1/2}\,, \qquad (3.18)$$

labeled as model I, gives similar predictions for the electroproduction cross sections. For the $N^*(1236)$ these models are clearly the same.

Although these two models give similar integrated cross sections (in which the initial helicities are summed incoherently), they do give different predictions for the helicity eigenamplitudes individually. Second, the enhancement factor determined using each of these models is different. In addition to its simplicity, model I has the advantage of being an approximation, although crude, to a many-channel calculation.

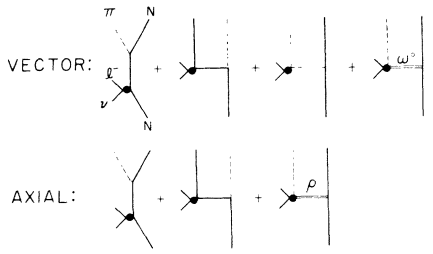

FIG. 5. Assumed excitation mechanism for the weak production of a pion-nucleon channel. The heavy dot indicates the current-current interaction.

Since our primary interest in calculating weak production is to predict the integrated cross section, we shall perform a model I calculation using Eq. (3.18). Although our electroproduction experience justifies this approach for the vector current (as a result of CVC), it is an assumption we make for the axial-vector amplitudes. Until accurate coincidence data at many values of k^2 and ϵ_1 become available, it is hoped that a simple model like this for $d\sigma/dk^2$ will suffice to explain and predict the experimental results.

Since we are performing a calculation based on the approximation of Eq. (3.18), we use the enhancement factors determined by comparing the model I electroproduction predictions with the SLAC data. The resulting values are given in Table I. Although the statistical uncertainties in these values for ϑ are fairly small, there is the possibility of a systematic error which is much larger. In separating the resonant from nonresonant events, the experimentalist is forced to assume a parametrization of the resonance shape, which is then fed into the computer. Different choices can give variations up to 30 or 40%[54] in normalization, but do not affect the dependence on k^2. In contrast, we recall that a factor-of-four uncertainty can be present when ϑ is calculated using models for the eigenphase shift.

Only five resonances are listed in Table I, since we found that they were sufficient to give the peaks observed in electroproduction. The spin-$\frac{1}{2}$ resonances are observed to be small in photoproduction[52] (implying small values for ϑ), and the model (as discussed in Sec. IV) predicts that $A^{\rm lhs}$ $(J = \frac{1}{2})$ will not grow relative to the higher-spin channels as k^2 increases. As a result, we attempt to predict weak production using the same levels given

TABLE I. Enhancement factors g obtained from comparison of electroproduction predictions (Refs. 11 and 12) and the most recent data from SLAC (Ref. 51). The relative enhancement of the two spin-$\frac{5}{2}$ levels was determined using photoproduction results from Ref. 52. Each resonance is labeled by its spin, parity, isospin, and energy.

State	g (GeV)
$\frac{3}{2}^+, \frac{3}{2}$ (1236)	10.8
$\frac{3}{2}^-, \frac{1}{2}$ (1520)	6.02
$\frac{5}{2}^-, \frac{1}{2}$ (1680)	0.20
$\frac{5}{2}^+, \frac{1}{2}$ (1688)	15.8
$\frac{7}{2}^+, \frac{3}{2}$ (1950)	11.9

in Table I.

IV. EXCITATION MECHANISM

The left-hand singularities of $A(W, k^2)$ are in general quite complicated. Fortunately, our model has the great advantage of not requiring direct knowledge of these singularities. Instead, all we need to know is the value of $A^{\text{lhs}}(W, k^2)$ for W near W_R. To approximate this value we build a model based on single-particle exchanges, which are dynamical singularities known to be present in $A(W, k^2)$. Other quantities (such as kinematic factors and the transformation coefficients[55] which define the eigenchannel) have known values for W near W_R. Interestingly, the reflection of the physical cut obtained when $W = -\sqrt{s}$ can be handled exactly and does not produce a resonant contribution for positive W.[56]

For the single-particle exchanges we obtain the pole-term contributions by evaluating Feynman diagrams with renormalized coupling constants, observed elastic form factors, and on-shell vertices. A partial-wave projection is then performed to obtain their contribution to A^{lhs}. In our previous calculation of electroproduction[10] we found that, in addition to pion and nucleon exchange, the inclusion of vector-meson exchange (a resonance treated as a single-particle exchange) was important; it was needed for the $N^*(1236)$ at large k^2 ($\gtrsim 0.5$ GeV^2) and for the higher resonances. Furthermore, we keep one nonpole term for the vector and one for the axial-vector current in order to explicitly guarantee current conservation or pion-pole behavior at small k^2.[57]

Since we are dealing with helicity eigenamplitudes, this evaluation of Feynman graphs and subsequent partial-wave projection must be performed for each contributing physical hadronic state. Fortunately, use of the approximation in Eq. (3.18),

$$A^{\text{lhs}}(W, k^2) \simeq a_{\pi N}^{\text{lhs}}(W, k^2)(\Gamma/\Gamma_{\pi N})^{1/2}, \tag{4.1}$$

reduces our task to a consideration of only the pion-nucleon final state. Below, we discuss the evaluation of the single-particle and vector-meson exchange contributions to $a_{\pi N}^{\text{lhs}}$. [$N^*(1236)$ exchange in the u channel was investigated for electroproduction[11] and found to be unimportant; we shall therefore not include it here.]

For the vector amplitudes, we use the conserved-vector-current theory of Feynman and Gell-Mann[6] to relate the matrix elements of the weak current to the electromagnetic. The isospin rotation accomplishing this is given by

$$\begin{aligned} J_\mu(\text{weak}) &= (J_\mu^{(1)} + iJ_\mu^{(2)})\cos\theta_c\,, \\ J_\mu(\gamma, \text{isovector}) &= J_\mu^{(3)}\,, \end{aligned} \tag{4.2}$$

with the superscripts denoting components in isospace. The factor $\cos\theta_c \simeq 0.975$ is the cosine of the Cabibbo angle,[58] which accounts for the fact that we are dealing with only the strangeness-conserving part of the weak current. (The Cabibbo angle also appears with the weak axial-vector current.) If we write this relation in terms of the isospin amplitudes given in Eq. (2.27), we obtain

$$A^{(\pm)}(\text{weak, vector}) = 2\cos\theta_c A^{(\pm)}(\text{electroproduction}). \tag{4.3}$$

The factor of 2 results from the choice of the isospin invariants[10] which for electroproduction have τ_3 rather than $\frac{1}{2}\tau_3$ where τ_+ appears in Eq. (2.27). After choosing our excitation model such that Eq. (4.3) is satisfied by A^{lhs}, we incorporate CVC by taking $D(W)$ to be the same as for electroproduction.

Figure 5 shows the particle exchanges used for the vector part of A^{lhs}. The nucleon and pion exchanges are needed together for current conservation, and the ω^0 contribution is conserved by itself. Since the ω^0 has odd G parity, it contributes here while the ρ contributes to the axial-vector current. [ϕ^0 exchange is expected to be unimportant since SU(6) and vector-meson dominance give $g_{\phi\pi\gamma} \approx 0$.[59]]

For the pion-nucleon coupling constant, we use

$$g_{\pi N}^2/4\pi = 14.6 \tag{4.4}$$

and describe the πNN vertex by the usual γ_5 coupling. At the current-nucleon-nucleon vertices we employ the known nucleon elastic, isovector form factors. Experimentally, we have the scaling law[30]

$$G_{Ep}(k^2) = G_{Mp}(k^2)/\mu_p = G_{Mn}(k^2)/\mu_n\,, \tag{4.5}$$

where μ_p and μ_n are total magnetic moments in nuclear magnetons. For the neutron electric form factor, a variety of scaling laws consistent with the elastic data were investigated[11] and found to

predict identical electroproduction cross sections for $k^2 \lesssim 1$ GeV^2. At larger k^2, differences became more pronounced, reaching 15% at $k^2 = 5$ GeV^2 for the $N^*(1236)$ and 25% for the $N^*(1520)$. In spite of these differences, the experimental electroproduction data at such large values of k^2 are not accurate enough to decide between the various scaling laws proposed. As a result, we now pick a convenient one,

$$G_{En}(k^2) = -k^2 G_{Mn}(k^2)/4m^2 , \tag{4.6}$$

which corresponds to $F_1^n(k^2) = 0$.

In order to assure current conservation regardless of the choice for the pion elastic form factor $F_\pi(k^2)$, we add the term

$$\bar{u}(p_2)\tfrac{1}{2}[\tau_\alpha, \tau_+]\, i\gamma_5 2g_{\pi N} \frac{F_\pi(k^2) - F_1^V(k^2)}{k^2}\, k_\mu u(p_1) \cos\theta_c , \tag{4.7}$$

to the contributions of the graphs in Fig. 5. Numerically, this term is unimportant, since k_μ contracts with the lepton operators to give a factor of the lepton mass (a factor of zero when the lepton masses are equal, as in electron scattering). In spite of its small size, we incorporate this term into our model to ensure a desired symmetry.

Having included this term, we are free to choose $F_\pi(k^2)$, subject only to charge conservation or

$$F_\pi(0) = 1 . \tag{4.8}$$

Since there is scanty experimental evidence for $F_\pi(k^2)$, we make an assumption motivated by simplicity and take

$$F_\pi(k^2) = F_1^V(k^2) . \tag{4.9}$$

In order to test our sensitivity to this assumption, we examined a variety of choices for $F_\pi(k^2)$. In all cases where $F_\pi(k^2)$ decreased asymptotically at least as rapidly as $G_{Ep}(k^2)$, we found that the cross section was insensitive to the choice. This is not surprising, since in this case the pion exchange is important only at small values of k^2 where F_π decreases smoothly from unity at $k^2 = 0$. On the other hand, if $F_\pi(k^2)$ decreases more slowly than $G_{Ep}(k^2)$ at large k^2, then the pion exchange becomes important at large k^2 and gives cross sections inconsistent with the electroproduction data (which show, as in Fig. 3, that the resonance decreases proportionately to the elastic). A similar argument also applies to the ω^0 form factor $F_{\omega\pi\gamma}(k^2)$. For example, the difference between using $F_2^V(k^2)/F_2^V(0)$ or $G_{Mp}(k^2)/\mu_p$ is at most a few percent ($k^2 < 5$ GeV^2) in the resonance cross section, but a choice behaving like $k^2 G_{Ep}(k^2)$ would give cross sections in disagreement with the data. Following simplicity, we have chosen

$$F_{\omega\pi\gamma}(k^2) = F_2^V(k^2)/F_2^V(0) . \tag{4.10}$$

For the coupling of the ω^0 to the nucleon, we use an interaction Lagrangian of the form

$$i g_{\omega NN} \bar{\psi}\gamma_\mu \psi \omega_\mu , \tag{4.11}$$

keeping only the charge coupling, since the nucleon isoscalar magnetic moment is small. For the $\omega\pi\gamma$ vertex we take[59] [and later use Eq. (4.3)]

$$V_{\omega\pi\gamma} = i g_{\omega\pi\gamma} \delta_{\alpha 3} \epsilon_{\mu\nu\rho\sigma} k_\mu e_\nu \omega_\rho q_\sigma , \tag{4.12}$$

where α is the isospin index of the emerging pion, ω_ρ the polarization of the ω^0, and e_ν the polarization of the current. The size of $g_{\omega\pi\gamma}$ can be determined from the electromagnetic decay of the ω, while the magnitude of $g_{\omega NN}$ is known only crudely. As a measure for this coupling, we introduce the quantity

$$\beta \equiv -\frac{g_{\omega\pi\gamma} g_{\omega NN}}{\frac{1}{2} g_{\pi N} F_2^V(0)}$$

$$\simeq -\sqrt{10}\, \frac{g_{\omega NN}}{g_{\pi N}}\, \frac{g_{\omega\pi\gamma}}{|g_{\omega\pi\gamma}|} . \tag{4.13}$$

For the electroproduction results, the value[10-12]

$$\beta = -6 \tag{4.14}$$

gave the best over-all k^2 dependence and corresponds to a $g_{\omega NN}$ in rough agreement with other determinations.[10] Having ascertained β from electroproduction, we no longer treat it as a parameter but as a predetermined quantity for use in our weak production calculation.

In addition to affecting the k^2 dependence, the sign of β has interesting consequences for the $J = \frac{1}{2}$ partial waves. In the 1520- and 1680-MeV regions there are also spin-$\frac{1}{2}$ resonances. At photoproduction,[52] we know that their contributions are small compared to the high-spin levels. As a result, we infer a small enhancement factor g. If β is negative (as above) the $A^{\text{lhs}}(J = \frac{1}{2})$ grow less rapidly with k^2 than do the higher-spin levels, and we can therefore consistently neglect the contributions from these $J = \frac{1}{2}$ levels. For a positive β, however, the $A^{\text{lhs}}(J = \frac{1}{2})$ would grow so rapidly with k^2 that the spin-$\frac{1}{2}$ levels would become prominent for $k^2 \gtrsim 0.5$ GeV^2 in spite of their small contribution at photoproduction. Although a direct measurement of resonance spins for $k^2 > 0$ is yet to come from coincidence experiments,[60] a negative value of β gains support from the SLAC data, whose peak locations and widths correspond nicely to our predictions[11] using only the higher-spin resonances.

Since ω^0 exchange only occurs in the vector amplitude (and since ρ exchange is unimportant in the axial-vector amplitude), the ratio A^{lhs}(axial vector)/A^{lhs}(vector) is sensitive to the choice of β.

Our predictions for weak production depend on this ratio, since[61]

$$A(W, k^2, \text{weak}) = A(W, k^2, \text{vector}) + A(W, k^2, \text{axial vector})$$
$$\simeq \frac{A^{\text{lhs}}(W, k^2, \text{vector})}{D(W)} \left[1 + \frac{A^{\text{lhs}}(W, k^2, \text{axial vector})}{A^{\text{lhs}}(W, k^2, \text{vector})}\right]. \quad (4.15)$$

As a result, different models for electroproduction, all of which agree with the electroproduction data, may not agree for weak production because of the term in brackets. In particular, the CERN data (discussed further in Sec. V) seem to support our model (with $\beta = -6$ as fixed by electroproduction), while Adler's calculation[18] (which does not contain ω exchange) falls far below these data for weak production of the $N^*(1236)$. For the small values of k^2 measured here, both calculations agree with electroproduction. A more detailed comparison of these two approaches is given in Appendix D. Interestingly, a hypothetical model based on positive β would do correspondingly worse for weak production.

For the axial-vector excitation function, we use the exchange graphs shown in the bottom part of Fig. 5. In contrast to the vector case, ρ exchange is present and pion exchange is forbidden by parity. (Appendix E gives the amplitude resulting from these graphs and the approximations discussed for both the vector and axial-vector cases.)

The axial-vector elastic form factors are defined by

$$\left(\frac{E_1 E_2 \Omega^2}{m^2}\right)^{1/2} \langle p_2 | J_{\mu 5}(0) | p_1 \rangle = i\bar{u}(p_2)[F_A(k^2)\gamma_5\gamma_\mu + iF_P(k^2)\gamma_5 k_\mu]\tau_+ \cos\theta_c u(p_1), \quad (4.16)$$

and we know from the neutron lifetime[62] that

$$F_A(0) = -1.23 \pm 0.01. \quad (4.17)$$

Observations of the elastic neutrino process

$$\nu + n \to p + l^- \quad (4.18)$$

include events at larger values of k^2 and indicate[31] that the axial-vector form factor is similar to the vector form factors. As a result, we choose

$$F_A(k^2) = F_A(0) G_{Ep}(k^2) \quad (4.19)$$

as our scaling law.

The pseudoscalar form factor $F_P(k^2)$, on the other hand, is very difficult to observe, since k_μ contracted into the lepton current gives a result proportional to the (small) lepton mass. From our discussion of the kinematics in Sec. II and Appendix C, we see that such terms are important only when k^2 is small (events near the forward direction). Proportionality to k_μ, on the other hand, has the particular asset of requiring the $F_P(k^2)$ term to be present in the divergence of the axial-vector current. As a result, a theory for this interesting current component will imply a choice for $F_P(k^2)$.

We shall adopt such a theory for the elastic reaction. It is commonly called the PCAC (partially conserved axial-vector current)[8] hypothesis and can be stated in several equivalent ways.[9] In one approach the divergence of the axial-vector current operator is equated with the pion interpolating field, assuming the extrapolation from $k^2 = 0$ to the pion mass shell is smooth. In the approach described below, we approximate a dispersion relation to be dominated by the pion pole (in k^2 as the dispersed variable) at small k^2.

Thus at small k^2 we have

$$2mF_A(k^2) - k^2 F_P(k^2) = \frac{2mF_A(0)\mu^2}{k^2 + \mu^2}, \quad (4.20)$$

where the residue has been evaluated by examining $k^2 = 0$. [This residue can also be given in terms of the pion-to-lepton-pair coupling constant. The relation of the residue to $F_A(0)$ was first obtained by Goldberger and Treiman[63] and has been confirmed to within 10%.] The term on the left-hand side of Eq. (4.20) occurs when the divergence of Eq. (4.16) is taken, and PCAC implies that the dispersion integral (plus any subtraction constants, usually assumed absent) occurring on the right-hand side of Eq. (4.20) can be neglected for small k^2. A pion pole occurs in the dispersion relation for $2mF_A - k^2 F_P$, since the pion has the same quantum numbers as the divergence of the axial-vector current. Since $F_A(k^2)$ is present for the other components of the axial-vector current, we know that the pion pole appears only in $F_P(k^2)$.

At larger values of k^2, a more general relation is needed. [Eq. (4.20) is only applicable for small k^2, meaning the order of μ^2.] As a result, we adopt Nambu's version of PCAC[8] and take

$$F_P(k^2) = 2mF_A(k^2)/(k^2 + \mu^2),$$
$$2mF_A(k^2) - k^2 F_P(k^2) = \frac{2mF_A(k^2)\mu^2}{k^2 + \mu^2}, \quad (4.21)$$

as our scaling law and its immediate consequence. Since $F_A(k^2)$ is smoothly varying for k^2 near zero (no nearby poles or cuts), this formulation contains the results of Eq. (4.20) as a special case. A further advantage of this approach is that when

$k^2 \gg \mu^2$ (a relation satisfied for most k^2's of interest in weak production, since the pion mass is small in comparison to the other relevant energies), then $2mF_A - k^2F_P$ is much smaller than $2mF_A$, indicating that the divergence of the current is insignificant in comparison with the other components.

For the inelastic reaction of resonance production, we are also interested in dominating the divergence of the axial-vector current by a pion pole. Unlike the elastic case discussed above, this presents some additional difficulties. First of all, PCAC has not been subjected to a conclusive experimental test for inelastic processes. Second, extrapolations or dispersion in k^2 may be affected by what is done with W and $k \cdot q$ as k^2 is varied. Third, the residue of the pion pole depends on the enhancement factor g as well as on approximations in A^{lhs}. We shall return to a discussion of the residue after showing how A^{lhs} can be chosen proportional to $(k^2+\mu^2)^{-1}$.

Since the contribution to A^{lhs} (axial-vector divergence) from the nucleon-exchange graphs is not proportional to $(k^2+\mu^2)^{-1}$, an additional piece must be added. Unfortunately, the ρ exchange cannot solve this problem, since it has the wrong isospin properties. Rather, we proceed somewhat analogously to the vector case and incorporate a nonpole term into our model. We add

$$g_{\pi N}\cos\theta_c \bar{u}(p_2)\frac{ik_\mu}{2m}F_P(k^2)(\tau_\alpha\tau_+ + \tau_+\tau_\alpha)u(p_1) \tag{4.22}$$

to the contribution of the nucleon-exchange graphs. Since this term is proportional to k_μ, it is unimportant numerically but may be noticeable when k^2 is of the order of m_l^2.

Having included this extra piece, we see from Appendix E that the nucleon-exchange contribution to A^{lhs} for the divergence of the current becomes explicitly proportional to $2mF_A - k^2F_P$. The remaining factors in this proportionality, such as $(2k\cdot q + W^2 - m^2)^{-1}$, depend on the other kinematic variables. If W^2 and $\cos\theta_{kq}$ are held fixed and if k^2 is small but variable, then E_1, k_0, k^*, and $k\cdot q$ are all approximately constant. Therefore, we take W and $\cos\theta_{kq}$ as fixed while k^2 is dispersed or extrapolated from the pion mass to zero. Then for small k^2 we have

$$\begin{aligned} A^{\text{lhs}}(\text{divergence component}) &= C(2mF_A - k^2F_P) \\ &= 2mF_A(0)\mu^2 C/(k^2+\mu^2)\,, \end{aligned} \tag{4.23}$$

where C is a constant readily calculated from Appendix E and the partial-wave projection. Although this expression is similar to Eq. (4.20), we cannot yet make any conclusions about pion-pole dominance of the axial-vector current since the full amplitude also contains $D(W)^{-1}$. After discussing the ρ-exchange contribution, we will return to analyze the residue of this pion pole.

In evaluating the ρ-exchange contribution, we used the ρ-π axial-vector vertex given by Segrè and Walecka[59] to obtain

$$\left(\frac{2\omega_q E_1 E_2 \Omega^3}{m^2}\right)^{1/2}\langle p_2 q^{(\text{out})}|J_{\mu 5}(0)|p_1\rangle_\rho^{\text{lhs}} = G_5^F F_{\rho\pi A}(k^2)(\tfrac{4}{3}\mu m_\rho)^{1/2}\cos\theta_c[(k-q)^2+m_\rho^2]^{-1}$$
$$\times\bar{u}(p_2)\tfrac{1}{2}[\tau_\alpha,\tau_+]\{\delta_{\mu\nu} - b(k^2)k_\nu q_\mu + c(k^2)k_\mu k_\nu\}[g_{1\rho NN}\gamma_\nu - g_{2\rho NN}\sigma_{\nu\lambda}(k-q)_\lambda]u(p_1)\,. \tag{4.24}$$

We thus have three form factors to determine. As in the case of ω^0 exchange for the vector part, we choose a particularly simple model:

$$\begin{aligned} &F_{\rho\pi A}(k^2) = F_A(k^2)/F_A(0)\,, \\ &b(k^2) = 0\,, \\ &c(k^2) = -(k^2+\mu^2)^{-1}\,. \end{aligned} \tag{4.25}$$

Since $c(k^2)$ occurs multiplied by k_μ, it contains the pion-pole contribution, and we are careful not to ignore it. The particular form for $c(k^2)$ given in Eq. (4.25) implies that the ρ-exchange contribution to the divergence of the current is proportional to

$$F_{\rho\pi A}(k^2)k_\mu[\delta_{\mu\nu} - k_\mu k_\nu/(k^2+\mu^2)] = k_\nu F_A(k^2)\mu^2/(k^2+\mu^2)\,. \tag{4.26}$$

For small k^2 and fixed W, $\cos\theta_{kq}$, the other factors in Eq. (4.24) are approximately constant. As a result, the ρ-exchange contribution to the divergence of the current behaves like the nucleon component in that it equals a constant times $(k^2+\mu^2)^{-1}$ at small k^2.

The coupling constant G_5^F appearing in Eq. (4.24) has been calculated by Segrè and Walecka[59] using quark-charge sum rules saturated by vector mesons. For a result, they obtain

$$(G_5^F)^2 = 12m_\rho/\mu \tag{4.27}$$

if $b(k^2)$ is zero. Using vector-meson dominance for the ρ-nucleon coupling constants, we obtain

$$\begin{aligned} &g_{1\rho NN} = F_1^V(0)\gamma_\rho\,, \\ &g_{2\rho NN} = F_2^V(0)\gamma_\rho\,, \end{aligned} \tag{4.28}$$

where γ_ρ is the ρ-γ coupling constant. Its value is known approximately from measurements of meson production from nuclei[64]:

$$\gamma_\rho^2/4\pi = 0.5-0.8\,. \tag{4.29}$$

In addition to knowledge of $(G_5^F)^2$ and $(\gamma_\rho)^2$, Eq. (4.24) requires knowledge of the sign of $G_5^F\gamma_\rho$. Fortunately, PCAC implies a definite choice for this sign, as a comparison with Adler's evaluation of the ρ-exchange contribution will show. In his calculation,[18] Adler considers a soft final pion ($q_\mu = 0$) and uses PCAC to relate this final pion to the divergence of the axial-vector current. After using current commutation relations, he obtains a value of the coupling which then gives, upon comparison with Eq. (4.24), the relation

$$(\tfrac{4}{3}m_\rho\mu)^{1/2}G_5^F\gamma_\rho/m_\rho^2 = -g_{\pi N}/mF_A(0)\,. \tag{4.30}$$

From this we determine that

$$G_5^F\gamma_\rho > 0\,, \tag{4.31}$$

since $F_A(0)$ is negative. Although we choose to use Eqs. (4.27)–(4.29) for the magnitudes of the coupling constants, we note that they are consistent with Eq. (4.30). More particularly, the value of G_5^F from Eq. (4.27) combined with Eq. (4.30) would imply

$$\gamma_\rho^2/4\pi = 0.44\,, \tag{4.32}$$

which is close to the lower limit in Eq. (4.29), the latter of which we chose as our value.

In the preceding discussion (and also in Appendix E) we have described our model for $A^{\rm lhs}$ in terms of particle exchanges, coupling constants, and elastic form factors. Furthermore, we have constructed $A^{\rm lhs}$ so that the vector current is explicitly conserved. For the divergence of the axial-vector current, we have explicit proportionality to $(k^2+\mu^2)^{-1}$ at small k^2 (W and $\cos\theta_{kq}$ held fixed). PCAC has been used in determining the elastic form factors and is yet to be discussed for the residue of the pion pole in $A^{\rm lhs}$.

The residue of the pion pole in our model can be compared with the PCAC prediction by looking at the cross section $d^2\sigma/dWdk^2$ for small k^2. Using the discussion in Appendix C, we see how this is related to the divergence of the axial-vector current. A partial-wave projection needs to be performed, but our predictions given in Sec. V are the results of such a projection. [We need the residue of $A(W,k^2)$ and not the residue of $A^{\rm lhs}$.] Finally, the pion-nucleon scattering data at the same W and in the same partial wave must be used for the comparison. For the $N^*(1236)$, the case of most immediate interest, our small k^2 amplitude is then found to be approximately a factor of 2 higher than the PCAC predictions (comparison made at $\epsilon_1 = 1$ GeV).

There are several possible explanations for such a discrepancy. First, there may be some problems with the $A^{\rm lhs}/D$ model at small k^2. In electroproduction[10-12] such a model had its most serious problems near $k^2 = 0$, and some other calculations[18-20] for the $N^*(1236)$ have gone so far as to build more detailed models in the small k^2 region. Such problems could arise if $A^{\rm lhs}$ did not vary slowly enough across the resonance for the approximations in Sec. III to apply. A direct examination of $A^{\rm lhs}$ does indicate a greater variation in W for small k^2 compared to large k^2. (We recall that for large k^2, $A^{\rm lhs}$ contains a cut intersecting the real axis near $W=m$. At small k^2 this cut is much shorter and is concentrated near the real axis.)

Another possibility is that $A^{\rm lhs}$ is inaccurate. Perhaps some of the approximations made for the ρ-exchange couplings or form factors need revising. Perhaps additional particle exchanges are needed for this current component. In comparing to the PCAC values, we are sensitive to only one current component. On the other hand, our model is designed to predict cross sections at larger k^2, where all the current components contribute. Indeed, it is possible to modify $A^{\rm lhs}$ so that the cross-section predictions (except the small k^2 limit) are scarcely altered while the divergence of the current is substantially changed. For this present calculation, we have refrained from adding such refinements to our model. When accurate experimental data at small k^2 become available, then it may be feasible to attempt a more sophisticated treatment of the small-k^2 region.

Yet another possibility is that $D(W_R)$ and therefore the enhancement factor g need to be changed. Since our present choice of g is supported by numerous electroproduction data and since it gives weak predictions in agreement with the CERN data discussed in Sec. V, we have confidence in its value. Thus, if the future neutrino data were to support the PCAC prediction, we would attribute the problem with our prediction to the possible causes discussed in the preceding paragraphs, and not to the value of g.

V. NUMERICAL RESULTS

We now proceed to present our results for the noncoincidence cross section. From Sec. II we have the expression

$$\frac{d^2\sigma}{dWdk^2} = \frac{W}{m^2}\,\frac{G^2}{8\pi}(K_1\tilde{W}_1 + K_2\tilde{W}_2 + K_3\tilde{W}_3)\,, \tag{5.1}$$

and Appendix B gives the coincidence cross section. The purely kinematic K_i are given in Eq.

(2.12). Although the properties of these K_i are discussed in Sec. II and Appendix C, we note here that when ϵ_1 is large compared to k^* and k_0^L, then K_1 and K_3 are small while K_2 is approximately constant. For k^2 near its minimum value, however, the situation is different, since K_2 approaches zero as k^2 decreases to its limit.

All the dependence upon ϵ_1 is contained in the K's, since the structure factors $\tilde{W}_i$ depend only on W and k^2. By using Eq. (2.24) we can obtain these structure factors from the helicity amplitudes. Our model, of course, predicts the resonant parts for the helicity eigenamplitudes, and therefore gives us predictions for the resonant parts of the $\tilde{W}_i$.[65] Conveniently, we may express these results in terms of the "resonance structure functions" $w_i(k^2)$ defined by

$$w_i(k^2) \equiv \frac{1}{m}\int dW \tilde{W}_i(W,k^2)_{\mathrm{Res}}. \tag{5.2}$$

In Table II our numerical predictions for $w_i/G_{Ep}{}^2$ are given for the resonances expected to be prominent in weak production. Although these values may increase slowly with k^2, there is a tendency for them to level off when k^2 becomes large. As a result, we predict that the resonance cross section $d\sigma/dk^2$ will behave like the elastic cross section at large k^2. In Figs. 3 and 4 we have seen a similar pattern for electroproduction.[66]

At very small values of k^2, on the other hand, w_1 and w_3 contain a large contribution from a term proportional to $k^{*2}m_l{}^2/k^4$. For the values of k^2 given in the table, this factor will be small for the electron-neutrino case but large for muon neutrinos. Since the final lepton has a finite rest mass, k^2 cannot decrease to zero but has a limit (at fixed W and ϵ_1) given by

$$k_{\min}{}^2 = m_l{}^2\frac{k_0^L}{\epsilon_1 - k_0^L} + O(m_l{}^4) \simeq m_l{}^2\frac{W^2 - m^2}{2m\epsilon_1 - W^2 + m^2}. \tag{5.3}$$

Our discussion relating to Eqs. (2.13)–(2.17) shows that the source of this peculiar kinematic behavior is the nonconservation of the axial-vector current. Furthermore, it is the large size of $k^{*2}m_l{}^2/k^4$ near the forward direction (k^2 near its minimum) which causes the cross section to be dominated by the divergence of the axial-vector current. Although w_1 and w_3 grow to a large finite limit as k^2 approaches its minimum, the cross section does not grow since K_1 and K_3 are both of order $m_l{}^2$, and K_2 is decreasing toward zero. These same comments pertain to $\tilde{W}_1$ and $\tilde{W}_3$ at any fixed W, and Appendix C investigates the behavior of $d^2\sigma/dWdk^2$ at small k^2 with an emphasis on the role played by the divergence of the axial-vector current.

Although the kinematic factors $K_{2,3}$ depend on W through k_0^L and k^*, this dependence is often quite weak. As a result, we may evaluate these factors at $W = W_R$ and obtain for each resonance

$$\frac{d\sigma}{dk^2} = \frac{W_R}{m}\frac{G^2}{8\pi}(K_1w_1 + K_2w_2 + K_3w_3). \tag{5.4}$$

When might K_2 and K_3 depend sensitively on W? Clearly, this can occur when there is a cancellation of the leading term in K_2 or K_3 by the one containing k_0^L. If ϵ_1 is large, such cancellations occur only very near the maximum and minimum values for k^2. For small ϵ_1 (near the threshold for producing the resonance), on the other hand, both terms in K_2 and K_3 are important over a wide range of k^2.

Another way of viewing this situation is to realize that this rapid variation in K_2 and K_3 occurs near the edge of the physical region. When the boundary of the physical region occurs in the region of the resonance, only part of the resonance peak is kinematically accessible, and Eq. (5.4) must therefore be modified.

Using Eq. (2.5) we find that the maximum W^2 possible at a fixed k^2 and ϵ_1 is given by

$$W_{\max}{}^2 = m^2 + 2m\epsilon_1 - k^2 - mm_l\left(\frac{k^2 + m_l{}^2}{2m_l\epsilon_1} + \frac{2m_l\epsilon_1}{k^2 + m_l{}^2}\right). \tag{5.5}$$

In terms of the lepton scattering angle (which we treat as a dependent variable[67]) this limit occurs at 0° if k^2 is smaller than $m_l(2\epsilon_1 - m_l)$ and at 180° if k^2 is larger than this amount. Equation (5.5) can also be solved to give the maximum and minimum values of k^2 for which a specified energy "$W_{\max}$" is in the physical region.

Integrating over energy then gives

$$\int_{W_0}^{W_{\max}} |A(W,k^2)|^2 dW \simeq \int_{W_0}^{W_{\max}} dW\,|A^{\mathrm{lhs}}(W,k^2)|^2\,|D(W)|^{-2}. \tag{5.6}$$

If $W_{\max}$ is near W_0, we cannot ignore the threshold factors present in A^{lhs}. Rather than evaluate A at all values of W, we approximate its threshold factors as follows:

$$A^{\mathrm{lhs}}(W,k^2) \approx \begin{cases} (q/q_R)^{l+1/2}A^{\mathrm{lhs}}(W_R,k^2), & W \le W_R \\ A^{\mathrm{lhs}}(W_R,k^2), & W \ge W_R. \end{cases} \tag{5.7}$$

Here l is the orbital angular momentum of the final pion and q_R is the c.m. three-momentum of the pion when $W = W_R$. For $|D(W)|^{-1}$ we follow the discussion in Sec. III and choose a symmetric Breit-Wig-

TABLE II. Resonance structure factors. Predictions for the integrated structure factors (defined in the text) are given for the resonances expected to be prominent in production by neutrinos incident on nucleons. For the isospin-$\frac{1}{2}$ levels (at 1520, 1680, and 1688 MeV) the target nucleon is taken as a neutron while for the isospin-$\frac{3}{2}$ levels (1236 and 1950 MeV) it is a proton. By using the expression in Eq. (2.28) and changing the sign of w_3 (except for those parts of w_3 dependent upon the lepton mass), the predictions for antineutrinos can be obtained. For all these levels the final state is a pure isospin state in the eigenchannel, with all decays therefore included in the sum. Furthermore, the results for the two spin-$\frac{3}{2}$ levels near 1680 MeV have been combined. Results are given for both electron and muon neutrinos. The square of the elastic proton form factor $G_{Ep}{}^2$ is divided out since it is the resultant ratio which our model calculates directly (and without making any assumptions about G_{Ep}).

k^2 (GeV^2)	lepton	$w_1/G_{Ep}{}^2$	$w_2/G_{Ep}{}^2$	$w_3/G_{Ep}{}^2$	$w_1/G_{Ep}{}^2$	$w_2/G_{Ep}{}^2$	$w_3/G_{Ep}{}^2$
			$N^*(1236)$			$N^*(1520)$	
0.001	electron	7.62	4.34	8.89	1.59	0.249	−0.282
0.005		7.49	4.45	8.70	1.55	0.259	−0.352
0.01		7.48	4.55	8.77	1.54	0.271	−0.354
0.05		7.44	4.80	9.37	1.46	0.351	−0.354
0.1		7.41	4.52	10.11	1.38	0.419	−0.357
0.3		7.32	4.53	12.03	1.49	0.587	−0.302
0.001	muon	5.50×10^3	4.34	1.10×10^4	1.56×10^3	0.249	3.11×10^3
0.005		2.00×10^2	4.45	3.86×10^2	55.6	0.259	1.05×10^2
0.01		50.8	4.55	89.4	13.57	0.271	21.8
0.05		8.75	4.80	10.94	1.86	0.351	+0.0567
0.1		7.66	4.52	10.34	1.49	0.419	−0.291
0.2		7.38	4.53	11.17	1.43	0.511	−0.336
0.3		7.34	4.53	12.04	1.51	0.587	−0.298
0.4		7.41	4.55	12.84	1.63	0.660	−0.223
0.5		7.53	4.59	13.52	1.76	0.730	−0.125
0.7		7.85	4.72	14.50	2.01	0.850	+0.110
1.0		8.39	4.88	15.56	2.28	0.968	+0.470
2.0		9.71	4.96	15.93	2.57	1.039	1.266
3.0		10.25	4.58	14.84	2.49	0.944	1.551
4.0		10.38	4.12	13.43	2.32	0.829	1.601
5.0		10.34	3.69	12.19	2.13	0.724	1.554
			$N^*(1680)+N^*(1688)$			$N^*(1950)$	
0.001	electron	1.082	0.120	−1.102	0.740	0.188	−0.142
0.005		1.040	0.124	−1.162	0.634	0.189	−0.357
0.01		1.025	0.129	−1.159	0.637	0.190	−0.357
0.05		0.924	0.169	−1.126	0.683	0.201	−0.312
0.1		0.814	0.213	−1.078	0.747	0.217	−0.250
0.3		0.626	0.301	−0.931	1.034	0.315	+0.0561
0.001	muon	1.40×10^3	0.120	2.78×10^3	4.85×10^3	0.188	9.69×10^3
0.005		49.3	0.124	92.9	1.68×10^2	0.189	3.26×10^2
0.01		11.8	0.129	18.6	37.6	0.190	67.7
0.05		1.30	0.169	−0.761	1.84	0.201	+0.903
0.1		0.927	0.213	−1.019	1.040	0.217	−0.0622
0.2		0.724	0.269	−0.991	0.969	0.261	−0.0783
0.3		0.647	0.301	−0.927	1.078	0.315	+0.0662
0.4		0.625	0.322	−0.863	1.218	0.377	+0.244
0.5		0.627	0.341	−0.795	1.369	0.442	0.448
0.7		0.668	0.371	−0.650	1.69	0.567	0.919
1.0		0.735	0.416	−0.401	2.19	0.733	1.76
2.0		0.906	0.502	+0.342	4.27	1.225	5.31
3.0		1.050	0.580	+0.888	6.74	1.75	8.93
4.0		1.183	0.647	1.237	9.22	2.24	12.02
5.0		1.268	0.690	1.435	11.08	2.54	14.09

ner shape normalized to correspond to the observed electroproduction enhancement factor.[68] Although Eq. (5.7) contains additional numerical approximations introduced into our calculation, we shall see that $W_{\max}$ is in the resonance region only for very small (or large) k^2, or for small ϵ_1.

For K_2 and K_3 we choose an average value for $W < W_{\max}$. By the mean-value theorem, this corresponds to evaluating these factors at some W_a below $W_{\max}$. The sharp drop near $W_{\max}$ is then accounted for by the fact that the integration region ends there. If ϵ_1 is large, K_2 and K_3 vary smoothly until W is very near $W_{\max}$, and we are therefore insensitive to the choice of W_a. On the other hand, when ϵ_1 is near its threshold for producing the resonance, the choice of W_a has a larger effect on the results. In presenting our predictions for $d\sigma/dk^2$, we shall indicate where these considerations are important and where Eq. (5.4) is suitable.

Rather than give the ratio to the elastic cross section, we shall give the inelastic cross section by itself. Later, we shall integrate over k^2. At this point we must therefore assume some form for $G_{Ep}(k^2)$. Our choice is the "dipole fit,"[30]

$$G_{Ep}(k^2) = (1 + k^2/0.71\ \text{GeV}^2)^{-2}. \tag{5.8}$$

In Fig. 6 we present our results for the $N^*(1236)$ resonance at a variety of incident neutrino energies. Consider first the curve for 1000 GeV. At this high energy, K_1 and K_3 are negligible compared to K_2, which in turn is approximately constant. As a result, this curve depends only on our predictions for $w_2(k^2)$. From Table II our calculation gives $w_2/G_{Ep}{}^2$ as approximately constant, explaining the proportionality of $d\sigma/dk^2$ to $G_{Ep}{}^2$.

Upon what aspects of our theory does the nearly constant value of $w_2/G_{Ep}{}^2$ depend? The A^{lhs}/D form of our model implies the dependence on k^2 is isolated from the hadronic scattering. Our particle-exchange model for A^{lhs} shows that the dependence on k^2 in the propagators is not important in this region, while the dependence introduced through the elastic form factors is important. If these form factors scale with respect to G_{Ep}, our model then predicts a slowly varying $w_2/G_{Ep}{}^2$. Dramatically different behavior would result, however, if such elastic form factors as F_π, $F_{\omega\pi\gamma}$, or F_A were to behave asymptotically like $k^2 G_{Ep}$.

Of course, $w_2/G_{Ep}{}^2$ is not exactly constant, and the variations of this quantity with respect to k^2 are more sensitive predictions of our model. Such variations depend on the details of the scaling laws assumed for the elastic form factors and upon the propagators in the particle-exchange graphs of Fig. 5. In order to test these predictions experimentally, we should compare with the observed $d\sigma/dk^2$ divided by the elastic cross section.

Fortunately, observations at large ϵ_1 provide a

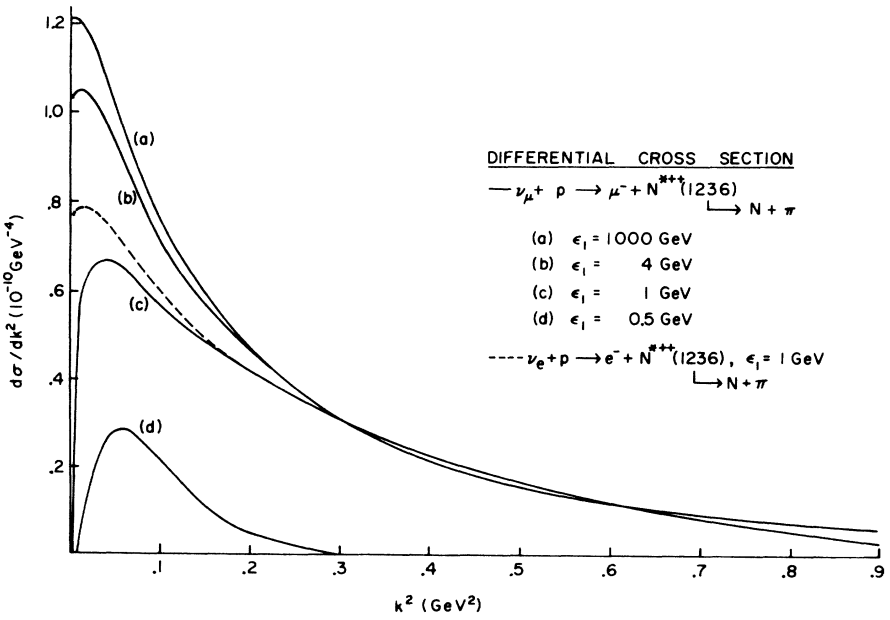

FIG. 6. Predictions for the differential cross section $d\sigma/dk^2$ for production of the $\frac{3}{2}^+, \frac{3}{2}$ (1236) resonance by neutrinos of various initial laboratory energies ϵ_1 incident on a proton target. Only the events containing a subsequent decay into a single pion plus a nucleon (pure isospin state) are included. All of these curves go to zero for small enough k^2 since the resonance is then outside the physical region. (The kinematic constraints on k^2 and W for fixed ϵ_1 are discussed in the text.) We recall that $1\ \text{GeV}^{-1} = 1.973 \times 10^{-14}$ cm.

convenient way of separating w_2 from w_1 and w_3. The necessary energy is not unreasonably high, either. From Fig. 6 we see that there is hardly any difference between $\epsilon_1 = 4$ and 1000 GeV for $k^2 \gtrsim 0.1$ GeV^2.

For smaller initial neutrino energies several changes occur. On the one hand K_1 and K_3 are larger, meaning that w_1 and w_3 have noticeable contributions. Furthermore, K_2 starts to decrease from its maximum value before k^2 is extremely small. Again the dominant feature at large k^2 is the elastic dependence, and the more sensitive predictions are given by the ratio of the cross section to $G_{Ep}{}^2$.

Since w_3 contains the vector–axial-vector interference, its value is particularly model-dependent. Unfortunately its direct observation is difficult. Either low-ϵ_1 data must be subtracted from high-ϵ_1 data (to cancel out the w_2 contribution) or neutrino data must be subtracted from antineutrino data (because w_3 changes sign, except at small k^2). Even if the variations of $w_3/G_{Ep}{}^2$ with k^2 cannot be observed, the average value of this function over a large range of k^2 is still a meaningful test of the theory (which depends, among other things, on which particle exchanges are present for the axial-vector in relation to the vector amplitudes).

From the curves in Fig. 6, we notice that the region $k^2 \lesssim 0.1$ GeV^2 is quite interesting. Due to the behavior of the elastic form factor, approximately 40% of the events are predicted to occur in this small-k^2 region. In addition to the fact that the curves turn over as a result of decreases in the K's, we note that 0.1 GeV^2 is only approximately ten times the square of the muon mass. Therefore, effects due to the nonzero mass of the lepton can be observed and used to isolate the divergence of the axial-vector current. The dashed curve in Fig. 6 shows the $\epsilon_1 = 1$ GeV result for electron neutrinos, and its deviation from the muon curve illustrates the contribution of the $m_l{}^2$ terms in w_1 and w_3 and also the dependence of K_i upon $m_l{}^2$.

From Eqs. (2.13)–(2.17) and the discussion in Appendix C, we see that for k^2 smaller than $m_l k^*$, the values of w_1, w_2, and w_3 are related by

$$\frac{2w_1 + w_3}{4w_2} = \frac{W_R{}^2}{m^2} \frac{m_l{}^2 k^{*2}}{k^4} [1 + O(k^2)]^2 . \tag{5.9}$$

Since PCAC predicts a value for $(2w_1 + w_3)k^4$ in the forward direction, this prediction can be tested to lowest order in k^2 either by measuring $2w_1 + w_3$ for small k^2 at small ϵ_1 or by measuring w_2 for small k^2 at large ϵ_1. (This is related to the idea that if ϵ_1 is large enough, the lepton mass must be insignificant.)

In addition to predicting the residue of the pion pole, PCAC also predicts that the k^2 dependence is indeed that of a pion pole, namely, that in Eq. (5.9):

$$O(k^2) = -\frac{1}{2} \frac{k^2}{k^2 + \mu^2} . \tag{5.10}$$

In order to test this prediction, it is necessary to measure $2w_1 + w_3$ rather than w_2 at small k^2. Since $2w_1 + w_3$ is proportional to $m_l{}^2$ at low k^2, a possible way to isolate it would be to compare production by electron and muon neutrinos. As Fig. 6 shows, there is approximately a 20% effect present for the $N^*(1236)$ at $\epsilon_1 = 1$ GeV.

Of course, such measurements of small effects in restricted regions of k^2 can be quite difficult experimentally, but the results would be very interesting. Using a model like ours, however, can provide some simplifications. For example, the results in Table II suggest averaging values of $d\sigma/(dk^2 G_{Ep}{}^2)$ rather than $d\sigma/dk^2$ in order to improve statistics. [For each event seen in a bubble chamber, k^2 and therefore $G_{Ep}(k^2)$ can be determined.] Since the $w_i/G_{Ep}{}^2$ vary slowly, our model can be used to suggest the kind of uncertainty to be expected from averaging over large-k^2 regions. Furthermore, we see the value of ϵ_1 beyond which the cross section is independent of ϵ_1 (making a large energy bin possible). For the $N^*(1236)$, events with $k^2 \gtrsim 0.1$ GeV^2 can be binned for $\epsilon_1 \gtrsim 4$ GeV, while $k^2 \gtrsim 0.2$ GeV^2 suggests binning the $\epsilon_1 \gtrsim 1$ GeV events.

For testing PCAC we see from Table II that the transverse parts of w_1 and w_3 are negligible for $k^2 \lesssim 0.02$ GeV^2. For w_2 a similar statement holds, although w_2 does not contain m_l; the transverse contribution can be neglected only if k^{*2}/k^2 is sufficiently large. A larger bin ($k^2 \lesssim 0.1$ GeV^2) may be used if comparison with electron neutrinos is possible, for then the transverse contribution is made to cancel. A model like ours may also be useful for inferring the electron-neutrino cross section from the muon-neutrino data at larger k^2. Finally, the average value over a small k^2 bin of the term in Eq. (5.10) can be detected if ϵ_1 is not too large [as determined by Eq. (5.3)], but measurement of its variation with k^2 would be extremely difficult.

Returning to Fig. 6, we see that at very small k^2 the curves turn abruptly and decrease to zero. It is in this region that part of the resonance is kinematically excluded and Eq. (5.4) is no longer valid. A few sample numbers for the $N^*(1236)$ are given in Table III. For $\epsilon_1 > 1$ GeV, substantial portions of the resonance are outside the physical region only for a very small range in k^2, meaning that we are hardly sensitive to the approximations of Eq. (5.7). For $\epsilon_1 = 0.5$ GeV, on the other hand, $W_{\max}$ is never far from the resonance region, and

TABLE III. Fraction of the area under the $N^*(1236)$ peak which is in the physical region.

k^2 (GeV^2)	Lepton	$\epsilon_1 = 0.5$ GeV	$\epsilon_1 = 1.0$ GeV
0.01	electron	0.83	0.95
0.05		0.79	0.95
0.1		0.68	0.95
0.01	muon	0.02	0.81
0.05		0.53	0.94
0.1		0.48	0.94

our approximations in averaging K_2 and K_3 may introduce errors up to 20–30% in this case. We note further that the relation in Eq. (5.5) for $W_{\max}$ depends on the lepton mass, and that for electron neutrinos $W_{\max}$ enters the resonance region at lower values of k^2 than for muon neutrinos.

In Figs. 7, 8, and 9, we give similar predictions for the other three resonances expected to be important. Indeed, at low k^2 there is a sharp threshold rise, followed by an interesting region below 0.1 GeV^2, and then by the large-k^2 region, where the elastic behavior is most apparent. Again, as ϵ_1 is increased, the curves approach an asymptotic limit which is independent of ϵ_1. In comparison with Fig. 6, higher values of ϵ_1 are required for the asymptotic limit since W_R is larger, and we need $\epsilon_1 \gg k_0^L$. In each figure the curve with lowest ϵ_1 shows a slower threshold rise and corresponds to a $W_{\max}$ present in the resonance region over a large range of k^2. For the higher neutrino energies, $W_{\max}$ is only in the resonance region at very small (or very large) values of k^2, as the abrupt rise indicates.

By integrating over k^2, we wash out many of the features predicted by our model, but are left with one useful comparison with the experimental data.

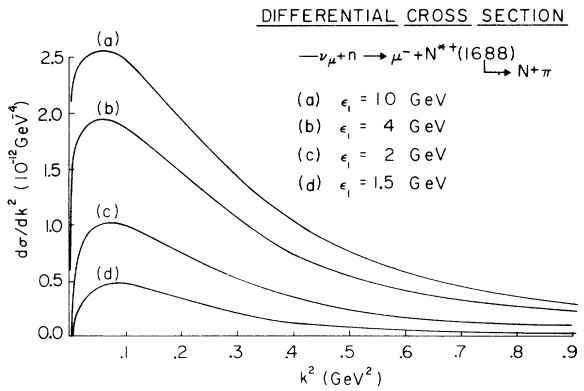

FIG. 8. Same as Fig. 6 except the sum for production of the $\frac{5}{2}^-, \frac{1}{2}$ (1680) and the $\frac{5}{2}^+, \frac{1}{2}$ (1688) levels produced from a neutron target is given.

In order to have this test, it is very important that we have not adjusted any parameters in this calculation, but have used enhancement factors previously determined by electroproduction. Figure 10 shows the results obtained by integrating the curves in Fig. 6. (Integrations were also performed at values of ϵ_1 not graphed in Fig. 6.) For this integration, cross sections at k^2 from 0.001 GeV^2 to 5 GeV^2 were considered, and we estimate the numerical error from the integration procedure to be less than 2%.

The shape of our predicted curve in Fig. 10 is easily explained. At small values of ϵ_1 the sharp rise is due to the fact that as ϵ_1 increases, the range of k^2 for which $W_{\max}$ is in the resonance region decreases. Also, K_2 is increasing toward its limit. After about 1-GeV neutrino energy, the asymptotic region is reached. Although $d\sigma/dk^2$ then hardly changes with increasing ϵ_1 (except for the small-k^2 region), the integral over k^2 could still conceivably grow with ϵ_1 since the range of

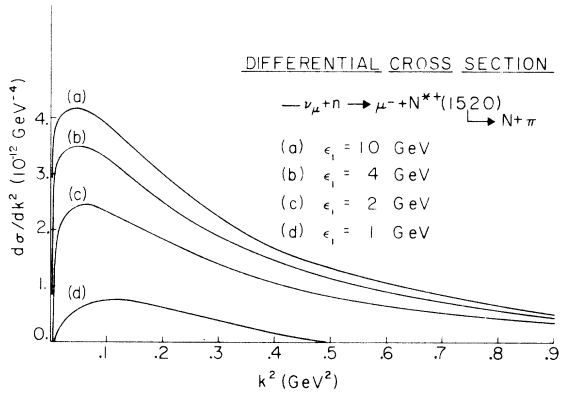

FIG. 7. Same as Fig. 6 except the $\frac{3}{2}^-, \frac{1}{2}$ (1520) level produced from a neutron target is given.

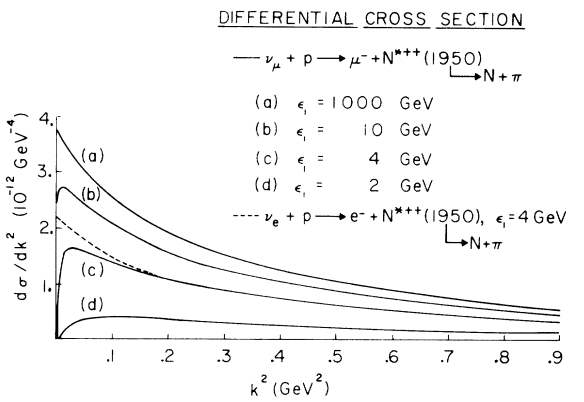

FIG. 9. Same as Fig. 6 except the $\frac{7}{2}^+, \frac{3}{2}$ (1950) level is given.

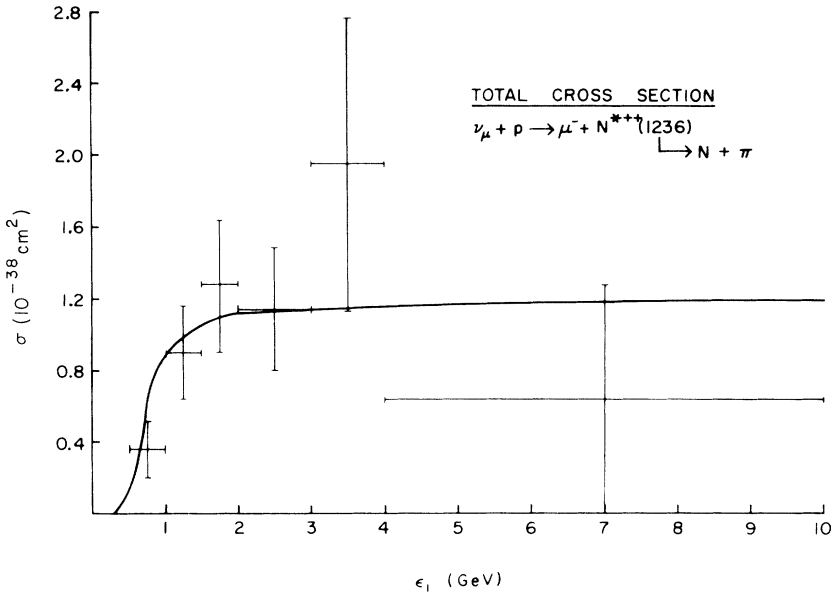

FIG. 10. Predicted total cross section for the $\frac{3}{2}^+, \frac{3}{2}$ (1236) level obtained by integrating the results in Fig. 6 over k^2 (at the indicated and at intermediate values of ϵ_1). Also shown are data points from the CERN experiment, Ref. 5.

k^2 increases ($k_{max}^2 \simeq 2m\epsilon_1$). Such growth does not occur, however, since the steep decrease of the elastic form factor and the proportionality of $d\sigma/dk^2$ to G_{Ep}^2 render this large-k^2 region insignificant. As a result, the predicted total cross section is fairly flat for $\epsilon_1 \gtrsim 1$ GeV and approaches an asymptotic value of approximately 1.2×10^{-38} cm^2. Even at large values of ϵ_1, most of the contribution comes from the region where $k^2 \lesssim 0.5$ GeV^2.

Figure 10 also shows the experimental measurements from CERN.[5] Although the error bars are large, the data do offer support for our results. [The distribution of the events in W is consistent with attributing them to the $N^*(1236)$.] In contrast, a fairly similar calculation by Adler[18] for the $N^*(1236)$, but not for the higher resonances, predicted a curve which rises monotonically to the much lower asymptotic value of 0.44×10^{-38} cm^2 [calculated at $\epsilon_1 = 4$ GeV using the same $F_A(k^2)$ as we did]. In Appendix D, we compare our calculation to Adler's and point out how differences in A^{lhs}, such as inclusion of ω exchange, and in enhancement factors can account for these widely differing predictions. (The two calculations agree for electroproduction at small $k^2 \lesssim 0.5$ GeV^2, but at larger values of k^2 Adler's predictions fall below ours and below the SLAC data.)

It should be a simple task for the experimentalists to bin their data for the $N^*(1236)$ region with $\epsilon_1 \gtrsim 1$ GeV and thereby obtain an accurate value to serve as a stringent test of our predictions. Since ϵ_1 is large, it is the predictions for w_2 which would be tested in this manner. Furthermore, since G_{Ep}^2 falls rapidly, it is the average of w_2/G_{Ep}^2 for $k^2 \lesssim 0.5$ GeV^2 to which the total cross section is sensitive. From Table II we notice that w_2/G_{Ep}^2 varies smoothly even for $k^2 \lesssim 0.02$ GeV^2 where terms related to the divergence of the axial-vector current take over. As discussed above, measurements in this small-k^2 region can be used to test PCAC. As our model stands now, the predicted values of $w_2(0)$ are larger than the PCAC values by a factor of nearly 4. If the data support PCAC, we then interpret this as an indication that our model needs refinements in the small-k^2 region. Possibilities for such refinements are discussed at the end of Sec. IV. Since the data in Fig. 10 support our predictions, such refinements would have to have little effect on w_2 for $k^2 \gtrsim 0.02$ GeV^2.

Total cross sections are similarly obtained for the higher resonances, and our predictions are

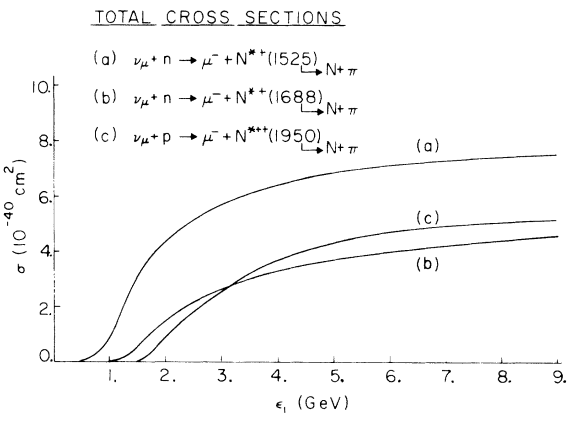

FIG. 11. Same as Fig. 10 except for the higher mass levels. No experimental data are available.

displayed in Fig. 11. As for the case of the $N^*(1236)$, these curves rise and level off towards an asymptotic value. The approach toward this asymptote is slower because the resonance masses are higher. Note that the isospin-$\frac{1}{2}$ levels cannot be excited by neutrinos from protons. Again, our predictions are meaningful since our calculation is an absolute calculation. Hopefully, experimental data will soon become available for these levels. In the meantime, our predictions are some indication as to what may be expected. By comparing with Fig. 10, we see that the total cross section for exciting these levels (at high ϵ_1) is approximately $1\frac{1}{2}$ orders of magnitude smaller than for the $N^*(1236)$.

VI. SUMMARY AND CONCLUSIONS

Having presented our theory and its predictions, we now take this opportunity to reexamine our goals and summarize what we have learned. In the process we shall review our important results and the major assumptions on which they depend. Finally, some possible refinements and extensions of our approach are suggested.

The nucleon resonances are of interest to us since they are manifestations of the structure of the nucleon. Our immediate goal is, then, to provide a calculation for the weak excitation of the $N^*(1236)$ (and contrast it with other existing calculations) and also to predict the excitation of higher-mass resonances (as yet unobserved and, to the best of our knowledge, uncalculated). Since our calculation does not include the adjusting of any parameters, we can meaningfully integrate over both W and k^2 and compare with the existing CERN data. As Fig 10 shows, this comparison is good, especially when we realize that a model such as Adler's[18] predicts a curve considerably below ours. The better statistics and different observations which should result from the neutrino experiments in progress or in planning[1-3] will provide more stringent tests of our model. These new data, however, are not expected to be able to test the details of the coincidence cross section, and we have accordingly designed our model to predict and explain the simpler noncoincidence results.

There is a variety of ways in which weak production provides us with more information than electroproduction. As Eq. (4.15) indicates, two models giving similar electroproduction predictions can differ greatly in weak production. Such is indeed the situation between our model and Adler's for the small-k^2 ($\lesssim 0.5$ GeV^2) production of the $N^*(1236)$. Even after integrating over k^2, the weak case neatly distinguishes these two models, provided the same $F_A(k^2)$ is used by both. At the root of this difference is our inclusion of ω^0 exchange as part of the vector-amplitude excitation mechanism. (Appendix D investigates these differences further.) Distinguishing the choices for the sign of the ω^0 coupling is also sensitively accomplished by the weak-production calculation, in contrast to the electroproduction calculation. So far, at least, electroproduction has the advantage of providing data on the $N^*(1236)$ at high k^2 and data on the higher resonances. These data do indeed add support to inclusion of the ω^0 with our choice of sign.

Since only isospin-$\frac{3}{2}$ resonances can be produced by neutrinos on proton targets, weak production provides a simple way of separating the contributions from certain overlapping resonances. In particular, by comparing proton and deuteron targets, we can check whether the $\frac{1}{2}^-$, $\frac{3}{2}$ (1650) resonance is indeed unimportant compared to the two spin-$\frac{5}{2}$ isospin-$\frac{1}{2}$ levels near 1688 MeV. Contributions from the recently discovered $\frac{3}{2}^-$, $\frac{3}{2}$ (1670) resonance can also be identified in this manner.

In the near-forward directions, or in the very-small-k^2 region, weak production allows us to observe the nonzero divergence of the axial-vector current. Measurements in this region can also check whether the vector current is conserved. As illustrated in Sec. V and Appendix C, our model is useful in estimating the relative size of the longitudinal and transverse amplitudes. Such knowledge then allows a determination of the region in k^2 over which the forward lepton theorem can be expected to hold. The very-small-k^2 region is also seen to be of interest because of the finite size of the muon mass.

Provided we choose a scaling law with asymptotic behavior, as in Eq. (4.21), PCAC has a generally negligible effect on our predictions. An exception occurs when k^2 is very small. In that case we can easily incorporate proportionality to the pion pole, but our absolute calculation cannot adjust the residue of this pole. Refinements in our model, however, can affect this residue which depends only on one helicity amplitude in one small kinematic region. CVC, on the other hand, has been thoroughly incorporated into this calculation, and must be considered as a possible source of discrepancies, but our model does not provide an unambiguous test of it. As mentioned above, the conservation of the vector current (one facet of the CVC theory) has a noticeable influence on the forward cross section.

Other special effects in weak production include the behavior as ϵ_1 becomes large (fixing k^2 and W). As shown in Sec. V, there exists an asymptotic region in which $d\sigma/dk^2$ is independent of ϵ_1. Furthermore, only the w_2 combination of helicity am-

plitudes is present in the cross section. In order to observe the vector–axial-vector interference, which is one of the interesting and sensitive features in such a calculation, lower values of ϵ_1 must be used. Although the existence of this asymptotic region follows from kinematic considerations, its onset is model-dependent since $K_1 w_1 + K_3 w_3$ must be small compared to $K_2 w_2$. When integrating over k^2, this asymptotic behavior for a resonance implies that the total cross section will rise and then flatten out as the asymptotic region is reached over most of the k^2 range. The proportionality of the resonance cross section to the sharply falling elastic form factor is needed here in order to guarantee that the high-k^2 region (which grows with increasing ϵ_1) is unimportant. If the sharp dependence on the elastic form factor is divided out, our predictions are the ones given in Table II and are seen to be smoothly varying in k^2. They depend on the approximations discussed in Sec. IV, being independent of the form assumed for $G_{Ep}(k^2)$.

Indeed, we have made many approximations in developing this model, some of which have important implications for our numerical results. Most basically we have assumed the $A^{\rm lhs}/D$ model of Eq. (1.4) for resonance production in a hadronic eigenstate. Although the justification of such a model is its ability to predict experimental data, there are some aesthetic and theoretical grounds for its choice. First of all, we note its simplicity: The k^2 dependence is isolated from the final-state enhancement function, the same model pertains for each current component, there is no integral over the physical cut, and it is linear in $A^{\rm lhs}$. In Sec. III we support this model on the grounds that it is an approximate solution to the Omnès equation and thereby incorporates unitarity. Such a discussion rests heavily on the fact that we are dealing with a resonance which is narrow enough for us to approximate $A^{\rm lhs}(W, k^2) \approx A^{\rm lhs}(W_R, k^2)$ as in Eq. (3.13). In calculating the cross sections, such an approximation is used again as illustrated in Eq. (1.7).

Our results are also sensitive to the model for $A^{\rm lhs}$ discussed in Sec. IV and based on pion, nucleon, and vector-meson exchange. In particular, the choice of exchange graphs, elastic form factors, and coupling constants have profound effects. We have seen for example that inclusion of ω^0 exchange with a coupling constant of particular sign and magnitude is important. By choosing the elastic form factors all proportional to $G_{Ep}(k^2)$, we produce the steep decrease with rising k^2 seen in Figs. 6–9. (The electroproduction data require this type of choice, at least for the vector amplitudes, within the framework of our model.) For the higher resonances, approximating $A^{\rm lhs}$ by only the pion-nucleon excitation function as in Eq. (3.18) is a big assumption which was seen to be justified in electroproduction.

CVC has been incorporated, since we have designed our model for $A^{\rm lhs}$(vector) in a manner comparable to electroproduction and have then chosen the same enhancement factors. By using these electroproduction enhancement factors, we are able to provide an absolute calculation which does not require any assumptions about the behavior of the hadronic phase shifts. We do assume, however, that the resonance occurs in only one hadronic eigenchannel. As discussed in Sec. III, our approach may contain a systematic error in the determination of the enhancement factors resulting from the choice of the phenomenological method used in separating the resonant events from the background in electroproduction.

If we choose to integrate over the resonance energy, some additional approximations are needed when k^2 or ϵ_1 is very small. These are discussed in Sec. V.

In terms of experimental results, our previous model did very well for electroproduction, and the present agreement with the CERN data looks encouraging. With limited statistics, our model indicates that large bins for σ and $d\sigma/(dk^2 G_{Ep}{}^2)$ are possible, and Sec. V indicates how small the bins in k^2 must be when testing PCAC. Hopefully the statistics will soon be good enough to compare high and low ϵ_1 at the same k^2, ν_e and ν_μ reactions, and ν and $\bar{\nu}$ reactions, thereby separating w_2 from w_1 and w_3. While many of our kinematic results are quite general, the model-dependent predictions pertain exclusively to the events containing a resonant final state.

Extensions and refinements of several kinds are possible for this calculation. On the one hand, we may refine our basic model of Eq. (1.4) by choosing a model more closely related to the Omnès solution in Eqs. (3.6) and (3.7). In particular, we may take advantage of the linearity of this solution and choose a more detailed model for the part of $A^{\rm lhs}$ which varies most rapidly across the resonance while keeping the simpler form of Eq. (1.4) for the remaining contributions. Such an approach has been taken by Adler[18] and others[19,20] for the pion-exchange contribution to the $N^*(1236)$. Their further assumptions then lead to a nonresonant enhancement of this contribution which helps the agreement with electroproduction data at low values of k^2. In a slightly different vein, by using Eq. (3.6) as the formulation of our model and by evaluating the energy integrals it contains, we could extend our calculation to the nonresonant amplitudes as well.

We may, on the other hand, refine our calculation by including more exchanges in A^{lhs} or by including more hadronic channels in the final state. Such extensions, however, possess the drawback of requiring the knowledge of more coupling constants or elastic form factors. Once detailed information is obtained from coincidence and polarization measurements, refinements of this type might become feasible. Inclusion of nonpole terms and off-shell vertices in A^{lhs} is also possible, and this has a particularly large effect in the spin-$\frac{1}{2}$ partial waves. As described previously, the spin-$\frac{1}{2}$ levels are not expected to be prominent.

In general, we are very encouraged that the simple model of Fig. 1, viewing resonance production as the excitation of an intermediate hadronic eigenstate which then rescatters to build up the resonance, has so far been supported by the data. Such a model incorporates unitarity above the $\pi\pi N$ threshold and is readily used for predicting the weak production of the $N^*(1236)$ and of the higher-mass resonances.

ACKNOWLEDGMENTS

The author wishes to thank J. D. Walecka for his continued interest and for useful discussions. He also appreciates the careful reading of the manuscript performed by M. J. Moravcsik and some stimulating questions posed by C. H. Llewellyn Smith.

APPENDIX A: CROSS-SECTION RELATIONS

In this appendix we derive the coincidence cross section for single-pion production by neutrinos. Special cases of this result are given in Sec. II and the partial-wave analysis of it is given in Appendix B. This is an original derivation which we feel is useful since the lepton mass is not ignored and the divergence of the current is carefully isolated from the other components.

The laboratory cross section for producing the πN final state is given by

$$\frac{d^4\sigma}{dW dk^2 d\Omega_q^*/4\pi} = \frac{W^2}{m^2}\frac{q}{4\pi\epsilon_1^{\,2}} L_{\mu\nu} J_\mu J_\nu^*, \tag{A1}$$

with J_μ related to the matrix elements of the hadronic current by Eq. (2.8). As previously, Ω_q^* is the solid angle of the emerging pion in the c.m. frame. The lepton part $L_{\mu\nu}$ results from the $V-A$ current-current theory of weak interactions and is given in Eq. (2.9). By summing the lepton spins, we then obtain

$$L_{\mu\nu} = 4G^2(k_{1\mu}k_{2\nu} + k_{1\nu}k_{2\mu} - k_1\cdot k_2\delta_{\mu\nu} + \xi\epsilon_{\alpha\beta\mu\nu}k_{1\alpha}k_{2\beta}), \tag{A2}$$

with $\xi = +1$ for neutrinos and -1 for antineutrinos. There is no averaging of initial spins since the neutrino has a definite helicity.

Since the partial-wave expansion will be performed in the c.m. frame of the final hadrons (the isobar rest frame), we shall expand $L_{\mu\nu}J_\mu J_\nu^*$ in that frame. In order to accomplish this task, we therefore need the c.m. components of $k_{1\mu}$ and $k_{2\mu}$ expressed in terms of W, k^2, and ϵ_1. Although this procedure can be extremely intricate and complicated, it is our purpose here to describe a method which avoids such difficulties.

Half the problem has already been solved, since we know the c.m. components of $k_\mu = k_{1\mu} - k_{2\mu}$. Using the coordinate axes given in Fig. 2, we see that $k_\mu = (|\vec{k}^*|\hat{e}_{k3}, ik_0)$ in this frame. For the remaining half of the problem we must analyze some independent linear combination of k_1 and k_2. Our choice,

$$r_\mu \equiv k_{1\mu} + k_{2\mu} - m_l^{\,2}k_\mu/k^2, \tag{A3}$$

is a particularly convenient one since

$$r\cdot k = 0. \tag{A4}$$

The square of this four-vector is readily evaluated from Eq. (A3) and is found to satisfy

$$-r^2 = (k^2 + m_l^{\,2})^2/k^2. \tag{A5}$$

Writing $r_\mu = (\vec{r}, ir_0)$ in the c.m. frame with $r_i \equiv \vec{r}\cdot\hat{e}_{ki}$, we readily see from Eq. (A3) and our choice of coordinate axes that

$$r_1 = 0. \tag{A6}$$

Thus we already have three constraints which the four c.m.-frame components of r_μ must satisfy. Although it is now possible to give an expression for r_2 in terms of the lepton scattering angle, it is far more convenient to express the fourth constraint in terms of a parameter, ϵ. Ultimately, we will relate this parameter to the independent kinematic variables.

As our definition, we choose

$$\epsilon \equiv r_2^{\,2}/(r_2^{\,2} - 2r^2), \tag{A7}$$

from which it follows that

$$r_2^{\,2} = (-r^2)2\epsilon/(1-\epsilon). \tag{A8}$$

From Eq. (A5) we see that r^2 is always negative, and we therefore have

$$0 \le \epsilon < 1. \tag{A9}$$

Using Eq. (A4), we find that the remaining components satisfy

$$\begin{aligned} \frac{k^2}{k^{*2}} r_0^{\,2} &= r_0^{\,2} - r_3^{\,2} \\ &= (-r^2)\frac{1+\epsilon}{1-\epsilon}, \\ \frac{k^2}{k_0^{\,2}} r_3^{\,2} &= (-r^2)\frac{1+\epsilon}{1-\epsilon}. \end{aligned} \tag{A10}$$

Later, we shall see that $r_2 \geq 0$ and $r_0 > 0$, implying that r_3 has the same sign as k_0.

Knowing the components of r_μ, we now return to the evaluation of $L_{\mu\nu}J_\mu J_\nu^*$. In terms of r_μ and k_μ, the lepton tensor of Eq. (A2) becomes

$$L_{\mu\nu} = 2G^2\Big\{r_\mu r_\nu + \frac{m_l^2}{k^2}(r_\mu k_\nu + k_\mu r_\nu) - k_\mu k_\nu\left(1 - \frac{m_l^4}{k^4}\right) + (k^2 + m_l^2)\delta_{\mu\nu} + \xi\epsilon_{\alpha\beta\mu\nu}k_\alpha r_\beta\Big\}. \tag{A11}$$

By working with the "C" and "D" components of the current defined in Eq. (2.15), we not only simplify the algebra but also isolate explicitly the divergence of the axial-vector current. Analogously, we define similar components for r_μ, and since $r \cdot k = 0$, we obtain the simple result

$$r_D = 0, \qquad r_C = r_0. \tag{A12}$$

The dot products present in $L_{\mu\nu}J_\mu J_\nu^*$ are conveniently expressed in terms of these components:

$$\begin{aligned} J\cdot k &= -k^2 J_D/k^*, \\ J\cdot r &= J_2 r_2 - \frac{k^2}{k^{*2}}J_C r_C, \\ J\cdot J^* &= |J_1|^2 + |J_2|^2 + \frac{k^2}{k^{*2}}|J_D|^2 - \frac{k^2}{k^{*2}}|J_C|^2, \end{aligned} \tag{A13}$$

where we have used the fact that both r_1 and r_D are zero. We may also use these components in the antisymmetric tensor if we take

$$\epsilon_{12CD} = -ik^2/k^{*2}. \tag{A14}$$

From here the expansion of Eq. (A1) in c.m.-frame components is a straightforward and relatively simple procedure. Using the spherical components of Eq. (2.14) for the transverse part of the current, we then obtain

$$\begin{aligned} \frac{d^4\sigma}{dW dk^2 d\Omega_q^*/4\pi} = \frac{G^2}{8\pi}(4q)\frac{k^2+m_l^2}{\epsilon_1^2}\frac{W^2}{m^2}\Big\{&\Big[|J^{+1}|^2 + |J^{-1}|^2 + \frac{m_l^2}{k^{*2}}(|J_C|^2 + |J_D|^2)\Big] \\ &+ \frac{\epsilon}{1-\epsilon}\frac{k^2+m_l^2}{k^2}\Big(|J^{+1}|^2 + |J^{-1}|^2 + 2\,\mathrm{Re}J^{+1*}J^{-1} + 2\frac{k^2}{k^{*2}}|J_C|^2\Big) \\ &+ \Big(\frac{1+\epsilon}{1-\epsilon}\Big)^{1/2}\Big(\xi|J^{-1}|^2 - \xi|J^{+1}|^2 + 2\frac{m_l^2}{k^{*2}}\mathrm{Re}J_C^*J_D\Big) \\ &+ \Big(\frac{k^2}{k^{*2}}\frac{\epsilon}{1-\epsilon}\Big)^{1/2}\Big[2\xi\,\mathrm{Im}J_C^*(J^{-1} - J^{+1}) + 2\frac{m_l^2}{k^2}\mathrm{Im}J_D^*(J^{+1} + J^{-1})\Big] \\ &+ \Big(\frac{1+\epsilon}{1-\epsilon}\Big)^{1/2}\Big(\frac{k^2}{k^{*2}}\frac{\epsilon}{1-\epsilon}\Big)^{1/2}\Big(\frac{k^2+m_l^2}{k^2}\Big)[2\,\mathrm{Im}J_C^*(J^{+1} + J^{-1})]\Big\}, \end{aligned} \tag{A15}$$

with $\xi = +1$ for neutrinos and -1 for antineutrinos. If desired, J_C and J_D can be replaced by expressions involving J_0 and J_3 by using Eq. (2.15). The various types of dependence on ϵ may now be labeled by separate kinematic variables such as those given in Eq. (2.12). By integrating over the pion c.m. angles as done in Appendix B, all the interference terms except for $J_C^*J_D$ drop out, and we readily obtain Eq. (2.13).

Our remaining task is to express ϵ in terms of known kinematical quantities. For r_2 we have

$$\begin{aligned} r_2 &= \vec{r}\cdot\hat{e}_{k2} \\ &= \vec{r}\cdot\hat{k}\times\frac{\vec{k}_2\times\vec{k}_1}{|\vec{k}_2\times\vec{k}_1|} \\ &= \frac{m}{W}\frac{2}{k^*}\epsilon_1\epsilon_2\beta\sin\theta. \end{aligned} \tag{A16}$$

Since r_2 and $\hat{e}_{k2}$ are unchanged by the transformation to the laboratory frame, we have expanded the dot products in the lab frame using Eq. (2.5) and (A3). Clearly, r_2 is always positive except for the extreme cases of forward and backward scattering when it is zero. Combining with Eq. (A8) then yields

$$\begin{aligned} \epsilon^{-1} &= 1 + \frac{W^2}{m^2}k^{*2}\frac{(-r^2)}{2\epsilon_1^2\epsilon_2^2\beta^2\sin^2\theta} \\ &= 1 + \frac{W^2}{m^2}\frac{2k^{*2}}{k^2}\frac{(1-\beta\cos\theta)^2}{\beta^2\sin^2\theta}. \end{aligned} \tag{A17}$$

In this form, we see that ϵ reduces to Hand's[22] "virtual-photon polarization" parameter if the lepton mass is ignored, which corresponds to taking the velocity β equal to one.

On the other hand, we may drive out the dependence on θ by using Eq. (2.5) to express $\beta^2\sin^2\theta$ in terms of k^2. The results of this procedure are shown in Eq. (2.12). For the dependence upon ϵ occurring in K_3, this method is somewhat cumbersome. By transforming to the lab frame and using Eqs. (A3) and (A4) we see that

$$\begin{aligned} \frac{r_0}{k^*} &= \frac{r_0^{\mathrm{lab}}}{|\vec{k}|_{\mathrm{lab}}} \\ &= \frac{m}{Wk^*}[(\epsilon_1 + \epsilon_2) - m_l^2(\epsilon_1 - \epsilon_2)/k^2]. \end{aligned} \tag{A18}$$

Combination with Eq. (A10) then leads to an expression for $(1+\epsilon)/(1-\epsilon)$ which does not involve θ. From Eq. (A18) we can also infer that r_0 is always positive.

Once we have suitable expressions for $\epsilon/(1-\epsilon)$

and $(1+\epsilon)/(1-\epsilon)$, as in Eq. (2.12), then Eq. (A15) shows that we have achieved our goal.

APPENDIX B: PARTIAL-WAVE DECOMPOSITION

We now give the result obtained by inserting the partial-wave expansion of Eq. (2.18) into the cross section in Eq. (A15). After summing over baryon spins and forming states of definite parity, we obtain an expression for the cross section in terms of the helicity amplitudes, which are defined in Sec. II. In the following, we restrict our attention to the case of a pion-nucleon final state. By integrating this result over the pion c.m. angles θ_{kq} and ϕ_{kq} (shown in Fig. 2), we then determine that the interference between the two longitudinal helicity amplitudes does not disappear and obtain the result used in Sec. II. In the following expression the dependence on θ_{kq} is contained in the functions h_1 through h_6, defined and discussed below. Also appearing is the parameter ϵ, which can be evaluated using Eq. (A17). Alternatively, Eq. (2.12) can be used to express the factors containing ϵ in terms of W, k^2, and ϵ_1.

A few simplifications in notation make the following expression easier to read and help to reveal its structure. First, we shall suppress the superscripts J^π and replace $J'^{\pi'}$ by a prime. Furthermore, since the (final) helicity of the pion-nucleon state is always $\frac{1}{2}$, we shall suppress it too. Thus, for example, a helicity amplitude like $T^{J^\pi}_{1/2,3/2}(W,k^2)$ will be denoted here by $T_{3/2}$, and $U^{J'^{\pi'}}_{1/2,C}(W,k^2)$ will become U'_C. Also, our dummy indices have been chosen in such a way that it is unprimed amplitudes which are complex conjugated.

For the partial-wave decomposition we then obtain

$$
\begin{aligned}
\frac{d^4\sigma}{dW dk^2 d\Omega_q^*/4\pi} = \frac{G^2}{8\pi}\frac{W^2}{m^2}\frac{k^2+m_l^2}{\epsilon_1^2}\frac{1}{k^*}
\times \sum_{JJ'\pi\pi'} \Bigg\{ & h_1\Bigg[\frac{2\epsilon}{1-\epsilon}\frac{k^2+m_l^2}{k^{*2}}\mathrm{Re}(T_C^* T'_C + U_C^* U'_C) \\
& + \frac{m_l^2}{k^{*2}}\mathrm{Re}(T_C^* T'_C + U_C^* U'_C + U_D^* U'_D) + \left(\frac{1+\epsilon}{1-\epsilon}\right)^{1/2}\frac{m_l^2}{k^{*2}}\mathrm{Re}(U_C^* U'_D + U_D^* U'_C)\Bigg] \\
& + h_2\Bigg[\left(1+\frac{k^2+m_l^2}{k^2}\frac{\epsilon}{1-\epsilon}\right)\mathrm{Re}(T^*_{1/2}T'_{1/2} + U^*_{1/2}U'_{1/2}) - \xi\left(\frac{1+\epsilon}{1-\epsilon}\right)^{1/2}\mathrm{Re}(T^*_{1/2}U'_{1/2} + U^*_{1/2}T'_{1/2})\Bigg] \\
& + h_3\Bigg[\left(1+\frac{k^2+m_l^2}{k^2}\frac{\epsilon}{1-\epsilon}\right)\mathrm{Re}(T^*_{3/2}T'_{3/2} + U^*_{3/2}U'_{3/2}) + \xi\left(\frac{1+\epsilon}{1-\epsilon}\right)^{1/2}\mathrm{Re}(T^*_{3/2}U'_{3/2} + U^*_{3/2}T'_{3/2})\Bigg] \\
& + 2h_4\cos 2\phi_{kq}\frac{\epsilon(k^2+m_l^2)}{(1-\epsilon)k^2}\mathrm{Re}(T^*_{1/2}T'_{3/2} + U^*_{1/2}U'_{3/2}) \\
& + 2h_4\sin 2\phi_{kq}\frac{\epsilon(k^2+m_l^2)}{(1-\epsilon)k^2}\mathrm{Im}(T^*_{1/2}U'_{3/2} + U^*_{1/2}T'_{3/2}) \\
& + 2h_5\sin\phi_{kq}\left(\frac{k^2}{k^{*2}}\frac{\epsilon}{1-\epsilon}\right)^{1/2}\Bigg[\left(\frac{1+\epsilon}{1-\epsilon}\right)^{1/2}\left(1+\frac{m_l^2}{k^2}\right)\mathrm{Re}(T_C^* T'_{1/2} + U_C^* U'_{1/2}) \\
& \qquad + \frac{m_l^2}{k^2}\mathrm{Re}U_D^* U'_{1/2} - \xi\,\mathrm{Re}(T_C^* U'_{1/2} + U_C^* T'_{1/2})\Bigg] \\
& + 2h_5\cos\phi_{kq}\left(\frac{k^2}{k^{*2}}\frac{\epsilon}{1-\epsilon}\right)^{1/2}\Bigg[\left(\frac{1+\epsilon}{1-\epsilon}\right)^{1/2}\left(1+\frac{m_l^2}{k^2}\right)\mathrm{Im}(T_C^* U'_{1/2} + U_C^* T'_{1/2}) \\
& \qquad + \frac{m_l^2}{k^2}\mathrm{Im}U_D^* T'_{1/2} - \xi\,\mathrm{Im}(T_C^* T'_{1/2} + U_C^* U'_{1/2})\Bigg] \\
& + 2h_6\sin\phi_{kq}\left(\frac{k^2}{k^{*2}}\frac{\epsilon}{1-\epsilon}\right)^{1/2}\Bigg[\left(\frac{1+\epsilon}{1-\epsilon}\right)^{1/2}\left(1+\frac{m_l^2}{k^2}\right)\mathrm{Re}(T_C^* T'_{3/2} + U_C^* U'_{3/2}) \\
& \qquad + \frac{m_l^2}{k^2}\mathrm{Re}U_D^* U'_{3/2} + \xi\,\mathrm{Re}(T_C^* U'_{3/2} + U_C^* T'_{3/2})\Bigg] \\
& - 2h_6\cos\phi_{kq}\left(\frac{k^2}{k^{*2}}\frac{\epsilon}{1-\epsilon}\right)^{1/2}\Bigg[\left(\frac{1+\epsilon}{1-\epsilon}\right)^{1/2}\left(1+\frac{m_l^2}{k^2}\right)\mathrm{Im}(T_C^* U'_{3/2} + U_C^* T'_{3/2}) \\
& \qquad + \frac{m_l^2}{k^2}\mathrm{Im}U_D^* T'_{3/2} + \xi\,\mathrm{Im}(T_C^* T'_{3/2} + U_C^* U'_{3/2})\Bigg]\Bigg\}. \qquad \text{(B1)}
\end{aligned}
$$

As always, ξ is +1 for neutrinos and −1 for antineutrinos. The summation in Eq. (B7) is unconstrained.

A glance at the preceding expression shows that the dependence on ϕ_{kq} is quite simple. The $\cos 2\phi_{kq}$ and $\sin 2\phi_{kq}$ terms come from the $(J^{+1})^*(J^{-1})$ interference while the $\cos\phi_{kq}$ and $\sin\phi_{kq}$ terms come from the longitudinal- (either "C" or "D" combination) transverse interference.

The dependence on θ_{kq}, on the other hand, is far more complicated. First, it is convenient to introduce a sign function:

$$S \equiv \begin{cases} +1 & \text{if} \quad \pi\pi' = (-1)^{J+J'+1}, \\ -1 & \text{if} \quad \pi\pi' = (-1)^{J+J'}. \end{cases} \tag{B2}$$

Then we have

$$\begin{aligned}
h_1 &= (J+\tfrac{1}{2})(J'+\tfrac{1}{2})\sum_{\lambda_2} d^J_{1/2\lambda_2} d^{J'}_{1/2\lambda_2}(\delta_{\lambda_2,1/2} + S\delta_{\lambda_2,-1/2}), \\
h_2 &= (J+\tfrac{1}{2})(J'+\tfrac{1}{2})\sum_{\lambda_2} d^J_{-1/2\lambda_2} d^{J'}_{-1/2\lambda_2}(\delta_{\lambda_2,1/2} + S\delta_{\lambda_2,-1/2}), \\
h_3 &= (J+\tfrac{1}{2})(J'+\tfrac{1}{2})\sum_{\lambda_2} d^J_{3/2\lambda_2} d^{J'}_{3/2\lambda_2}(\delta_{\lambda_2,1/2} + S\delta_{\lambda_2,-1/2}), \\
h_4 &= (J+\tfrac{1}{2})(J'+\tfrac{1}{2})\sum_{\lambda_2} d^J_{-1/2\lambda_2} d^{J'}_{3/2\lambda_2}(\delta_{\lambda_2,1/2} + S\delta_{\lambda_2,-1/2}), \\
h_5 &= (J+\tfrac{1}{2})(J'+\tfrac{1}{2})\sum_{\lambda_2} d^J_{1/2\lambda_2} d^{J'}_{-1/2\lambda_2}(\delta_{\lambda_2,1/2} + S\delta_{\lambda_2,-1/2}), \\
h_6 &= -(J+\tfrac{1}{2})(J'+\tfrac{1}{2})\sum_{\lambda_2} d^J_{1/2\lambda_2} d^{J'}_{3/2\lambda_2}(\delta_{\lambda_2,1/2} + S\delta_{\lambda_2,-1/2}),
\end{aligned} \tag{B3}$$

where $d^J = d^J(-\theta_{kq})$. From these expressions we readily see that

$$\begin{aligned}
\tfrac{1}{2}\int_{-1}^{1} d(\cos\theta_{kq}) h_{1,2,3} &= (J+\tfrac{1}{2})\delta_{J,J'}\tfrac{1}{2}(1+S) \\
&= (J+\tfrac{1}{2})\delta_{J,J'}\delta_{\pi,\pi'}.
\end{aligned} \tag{B4}$$

Furthermore, from the properties of the rotation matrices, we can easily ascertain that h_1, h_2, $h_3/\sin^2\theta_{kq}$, $h_4/\sin^2\theta_{kq}$, $h_5/\sin\theta_{kq}$, and $h_6/\sin\theta_{kq}$ are polynomials in $\cos\theta_{kq}$ with only even or odd powers occurring. For $S=+1$ the degree of these polynomials (the highest power of $\cos\theta_{kq}$) is

$$\begin{aligned}
&\deg(h_1, h_2) = J + J' - 1, \\
&\deg\left(\frac{h_3}{\sin^2\theta_{kq}}, \frac{h_4}{\sin^2\theta_{kq}}\right) = J + J' - 3, \\
&\deg\left(\frac{h_5}{\sin\theta_{kq}}, \frac{h_6}{\sin\theta_{kq}}\right) = J + J' - 2.
\end{aligned} \tag{B5}$$

When, on the other hand, $S=-1$, then the leading term has one additional power of $\cos\theta_{kq}$. In order to find the coefficients in these polynomials, we can rewrite Eq. (B3) in terms of derivatives of Legendre polynomials.

Since h_1 through h_6 are finite for all values of θ_{kq}, we know that when $\sin\theta_{kq}=0$, the functions h_3 through h_6 must vanish. Thus, the points $\theta_{kq}=0$ are very special, for the cross section greatly simplifies. Such observations also apply to electroproduction coincidence cross sections (where the same h's occur); the implications of this are discussed by Pritchett and Zucker.[33]

APPENDIX C: FORWARD LEPTON THEOREM

When k^2 is near its minimum value or, equivalently, when the final lepton emerges near the forward direction, the weak cross section is proportional to the divergence of the axial-vector current. Adler[7] was the first to point this out. In this Appendix we show how this "forward lepton theorem" is a consequence of the discussion in Sec. II. As part of this derivation, we shall see where approximations are made and what kind of model-dependent justifications are needed. After investigating the exact forward limit, we shall turn our attention to the more intricate behavior near the forward direction and to the problem of determining the kinematic region in which the theorem holds.

In the forward direction ($\theta=0$), we see from Eq. (2.5) that k^2 has its minimum value while $m_l^2 k^{*2}/k^4$ is large. Keeping the leading term in powers of m_l^2, we obtain the following forward limits:

$$\begin{aligned}
k^2 &= 2\epsilon_1\epsilon_2(1-\beta) - m_l^2 \\
&\simeq \frac{\epsilon_1-\epsilon_2}{\epsilon_2} m_l^2 = \frac{k_0^L}{\epsilon_1 - k_0^L} m_l^2, \\
W^2 k^{*2} m_l^2/m^2 k^4 &\simeq \frac{\epsilon_2}{\epsilon_1-\epsilon_2}\left[1 + \frac{\epsilon_2(\epsilon_1-\epsilon_2)}{m_l^2}\right] \\
&\simeq \frac{\epsilon_2^2}{m_l^2} = \frac{(\epsilon_1 - k_0^L)^2}{m_l^2}, \\
k_0^L &\simeq (W^2 - m^2)/2m, \\
\tfrac{1}{2}K_1 &= K_3 \\
&= (k^2 + m_l^2)/\epsilon_1^2 \\
&\simeq m_l^2/\epsilon_1\epsilon_2.
\end{aligned} \tag{C1}$$

The limit for K_2 is exactly zero.

Employing these results in Eqs. (2.11) and (2.13) then gives us the cross section in this limit:

$$\frac{d^2\sigma}{dW dk^2} \simeq \frac{G^2}{8\pi}\frac{W^2}{m^2}\frac{m_l^2}{\epsilon_1\epsilon_2}(4q)\int \frac{d\Omega_q^*}{4\pi}\left[(1+\xi)|J^{-1}|^2 + (1-\xi)|J^{+1}|^2 + \frac{m^2}{W^2}\frac{\epsilon_2^2}{m_l^2}\left|\frac{k^2}{k^{*2}}J_C + \frac{k^2}{k^{*2}}J_D\right|^2\right]. \tag{C2}$$

Had we taken the limit of the coincidence cross section in Eq. (A15), we would have obtained the same result but with the integral removed. The components of J_μ are defined in Eqs. (2.14) and (2.15). From Eq. (C2) it is apparent that J^{-1} contributes to neutrino processes while J^{+1} pertains to antineutrino reactions, in accordance with angular momentum conservation in the forward direction.

The expression in Eq. (C2) contains more than the divergence of the axial-vector current, and we make some approximations based on the fact that m_l^2 and k^2 are small compared to ϵ_2^2 and k^{*2}. In contrast to the approximations in Eq. (C1), which are purely kinematic, neglecting the terms of higher order in k^2 or m_l^2 in Eq. (C2) makes an assumption about the sizes of the matrix elements of the hadronic current. For example, if J^{-1} were much larger than $k^2 J_D/k^{*2}$, it would not be reasonable to neglect the transverse contribution in Eq. (C2). Away from the forward direction, k^2 is no longer of the order of m_l^2, and the model-dependent considerations become extremely important in approximating the cross section. First, we shall restrict our attention to the forward limit and make the approximations corresponding to keeping terms of the lowest order in m_l^2 or k^2.

From Eq. (2.15) we see that the combinations $k^2 J_C/k^{*2}$ and $k^2 J_D/k^{*2}$ are indeed of order unity when k^2 is small. If the current is conserved, however, then J_0 and J_3 tend to cancel, implying that J_C by itself is of order unity. As a result, $|k^2 J_C/k^{*2}|^2$ is of order k^4 for a conserved current. From Eq. (2.24) or Appendix B, we see there is no interference between the longitudinal vector and longitudinal axial-vector components. Thus, for a conserved vector current, we have

$$\left|\frac{k^2}{k^{*2}}J_C+\frac{k^2}{k^{*2}}J_D\right|^2=\frac{k^4}{k^{*4}}|J_C(\text{vector})|^2+\left|\frac{k^2}{k^{*2}}J_{C5}+\frac{k^2}{k^{*2}}J_{D5}\right|^2\approx\left|\frac{k^2}{k^{*2}}J_{C5}+\frac{k^2}{k^{*2}}J_{D5}\right|^2. \tag{C3}$$

The subscript 5 indicates the axial-vector piece. If, on the other hand, the vector current were not conserved, it would contribute as the axial-vector in the forward direction.

Our next approximation is to neglect the transverse contributions because $m^2\epsilon_2^2/W^2 m_l^2$ is a large number. Thus we take

$$2|J^{\mp1}|^2\ll\frac{m_l^2 k^{*2}}{k^4}\left|\frac{k^2}{k^{*2}}J_{C5}+\frac{k^2}{k^{*2}}J_{D5}\right|^2\approx\frac{m^2}{W^2}\frac{\epsilon_2^2}{m_l^2}\left|\frac{k^2}{k^{*2}}J_{C5}+\frac{k^2}{k^{*2}}J_{D5}\right|^2, \tag{C4}$$

using J^{-1} for neutrinos and J^{+1} for antineutrinos.

Let us now consider the small-k^2 behavior of $k^2 J_{C5}$ and $k^2 J_{D5}$. Since the latter contains a pion pole, it is expected to vary noticeably between the minimum value of k^2 and the unphysical value of $k^2=0$. (For electron neutrinos, the minimum k^2 is so much smaller than the pion mass squared that this variation can be ignored.) Other contributions to this component, as well as all the contributions to the C component, are taken as approximately constant. Since $k^2 J_C$ and $k^2 J_D$ have the same limit as k^2 goes to zero [see Eqs. (2.15) and (2.17)], we then take

$$\begin{aligned}\frac{k^2}{k^{*2}}J_{C5}&\approx\frac{k^2}{k^{*2}}J_{C5}\Big|_{k^2=0}\\&=\frac{k^2}{k^{*2}}J_{D5}\Big|_{k^2=0}\\&=-\frac{1}{k^*}J\cdot k\Big|_{k^2=0},\\\frac{k^2}{k^{*2}}J_{D5}&\simeq\frac{k^2}{k^{*2}}J_{D5}\Big|_{k^2=0}\frac{\mu^2}{k^2+\mu^2}\\&=-\frac{1}{k^*}J\cdot k\Big|_{k^2=0}\frac{\mu^2}{k^2+\mu^2},\\\left|\frac{k^2}{k^{*2}}J_{C5}+\frac{k^2}{k^{*2}}J_{D5}\right|^2&\simeq\frac{1}{k^{*2}}|J\cdot k|_{k^2=0}^2\left(1+\frac{\mu^2}{k^2+\mu^2}\right)^2.\end{aligned} \tag{C5}$$

We have also used PCAC by assuming $J\cdot k$ is proportional to a pion pole rather than to a constant plus a pion pole. Our model for these current components will give an indication how much they vary as they are extrapolated to $k^2=0$.

Putting all these approximations together then yields the forward cross section

$$\frac{d^2\sigma}{dW dk^2}\simeq\frac{G^2}{8\pi}\frac{\epsilon_2}{\epsilon_1}(4q)\times\int\frac{d\Omega_q^*}{4\pi}\frac{4}{k^2}|J\cdot k|_{k^2=0}^2\left(1-\frac{1}{2}\frac{k^2}{k^2+\mu^2}\right)^2. \tag{C6}$$

By inserting the minimum value of k^2 and equating $W^2 k^{*2}/m^2$ with k_0^{L2} (to lowest order in m_l^2), we obtain Adler's[7] result. From here, it is possible to use PCAC and relate $J\cdot k$ to observed pion-nucleon cross sections.

Since the leading term in the forward cross section is zeroth order in m_l^2, it is possible to obtain this same limit by setting m_l equal to zero at the very beginning (as Adler did originally). Then k^2, K_1, and K_3 would go to zero, with K_2 remaining large. Since $\tilde{W}_2$ contains J_C but not J_D, taking the limit in that fashion does not produce the $k^2/(k^2+\mu^2)$ term in Eq. (C6). In order to obtain this term, which he called the "lepton mass corrections," Adler then had to go through a more detailed derivation.

Nevertheless, our derivation here has many advantages. First of all, it provides this "lepton mass correction" term in an evident fashion. Second, it shows in Eqs. (C1) and (C3)–(C5) the other approximations implicit in taking only the leading order in m_l^2. Furthermore, the results of our model as given in Table II can be used to evaluate the accuracy of each of these approximations (for small k^2 near, as well as in, the forward direction). For example, for the $N^*(1236)$ and ϵ_1 equal to 1 GeV, the muon-electron difference is a 20% effect while approximations in the second line of Eq. (C1) and in Eq. (C4) each ignore about 5% of the cross section.

Since experiments measure events over finite angular regions, a very interesting question is the extent in θ or k^2 over which these approximations are valid. In answering these questions we need to know the exact kinematics and to have a model for the matrix elements of the hadronic current. Our calculation achieves both these goals. By referring to Eqs. (2.5) and (2.12), the kinematics can be exactly evaluated. From Table II, the longitudinal and transverse parts can be compared (by contrasting the muon-neutrino and electron-neutrino cases) and their variation with k^2 can be seen. Although conclusions about the size of the k^2 region where Eqs. (C4)–(C6) hold depend on W and ϵ_1, some general comments can be made, and some specific examples are given in Sec. V.

In general, the k^2 region is still small enough for the variation in $k^2 J_C$ to be neglected, particularly if we use the values of $k^2 J_C$ and $J_D k^2(k^2+\mu^2)$ at the middle of our bin rather than at k^2 extrapolated to zero. As k^2 increases, K_2 grows extremely rapidly while $K_1 m_l^2 k^{*2}/k^4$ decreases. As a result, we obtain important contributions from the $k^2 J_C$ term present in $\tilde{W}_2$. Thus we again compare longitudinal to transverse and need to approximate

$$2\frac{k^{*2}}{k^2}\left|\frac{k^2}{k^{*2}}J_{C5}\right|^2 \gg |J^{+1}|^2+|J^{-1}|^2 . \tag{C7}$$

Since $\tilde{W}_2$ does not contain J_D, the pion-pole term is further suppressed. It therefore seems advisable to consider the J_C and J_D terms separately (and their interference separately, too) and integrate each over the small-k^2 region using the exact kinematics. The boundary of this region is determined from Eqs. (C4) and (C7), which contain model-dependent approximations. Although the size of ϵ_1 is important in determining where the rapid growth of K_2 occurs, we note that Eqs. (C4) and (C7) are independent of ϵ_1 when they are viewed as depending on k^2 at fixed W.

APPENDIX D: COMPARISON WITH ADLER'S APPROACH

In this Appendix we compare our approach to that of Adler,[18] who has also calculated the weak production of the $N^*(1236)$ using a dynamical model based on dispersion relations. Although these two models agree for the low-k^2 ($\lesssim 0.5$ GeV^2) electroproduction of the $N^*(1236)$, they differ by over a factor of 2 in weak production for the same k^2 region. In addition to explaining this difference, we shall also compare the general approaches of the two calculations and the reasons given to support each model.

The calculations have different goals. Adler, on the one hand, investigates the $N^*(1236)$ and the nonresonant partial waves at low energies, thereby attempting to avoid the difficulties present above the $\pi\pi N$ threshold. On the other hand, we are interested in the higher resonances as well as the $N^*(1236)$. As a result, we consider the hadronic inelasticities and have built our model in terms of the helicity eigenamplitudes discussed in Sec. III. We do not, however, treat the nonresonant partial waves. Even though the $N^*(1236)$ can be considered as entirely in the pion-nucleon channel, considerations about the hadronic physics at higher energies do enter through the final-state enhancement function in Eq. (1.6), which contains an integral over all values of W. In our examination of how the two models treat the $N^*(1236)$, we shall see the role played by the asymptotic behavior of the hadronic scattering.

Using the definition of $X(W)$ which is given in Eq. (3.6), we can state Adler's model for the $N^*(1236)$ amplitudes as

$$A(W,k^2)\simeq \frac{X(W)}{X(m)}A^B(W,k^2)\left[1+\frac{a(k^2)^2}{(W-m)(W_R-m)}\right]. \tag{D1}$$

Here A^B is Adler's version for $A^{\rm lhs}$, which differs from ours. [We shall avoid using the notation $D(W)$ since Adler's D is proportional to $X(W)$ and ours equals X^{-1}.] The function $a(k^2)$ is given by Adler in his paper and is small when k^2 is small. Although Adler chooses a different model for the pion-exchange contribution to A^B, the result given above is used for the dominant contribution and is therefore the one of interest to us here.

The similarities to our model,

$$A(W,k^2)\simeq X(W)A^{\rm lhs}(W,k^2), \tag{D2}$$

are apparent. Since the $a(k^2)$ term is not important for small k^2, the main difference in the form of these two expressions is the presence of the factor $X(m)^{-1}$ in the former. [We recall that $X(W_0)^{-1}$ equals unity by definition.] Thus, even if we both were to use the same models for $X(W)$ and had $A^{\rm lhs}=A^B$, the two calculations would have similar k^2 and W behaviors but different absolute normalizations. Since

$$\frac{X(W)}{X(m)} = \exp\left[\frac{W-W_0}{\pi}\int_{W_0}^{\infty}\frac{\xi(W')dW'}{(W'-W_0)(W'-W-i\epsilon)} - \frac{m-W_0}{\pi}\int_{W_0}^{\infty}\frac{\xi(W')dW'}{(W'-W_0)(W'-W-i\epsilon)}\right]$$

$$= \exp\left[\frac{W-m}{\pi}\int_{W_0}^{\infty}\frac{\xi(W')dW'}{(W'-m)(W'-W-i\epsilon)}\right], \tag{D3}$$

we see that the presence of $X(m)$ results from the fact that Adler used a final-state enhancement function subtracted at m rather than at W_0. A rough estimate, using the model for the eigenphase shift discussed in Ref. 11, indicates that $X(m)$ has a value of less than $\frac{1}{2}$. Since we intend to integrate over the resonance, such factors affecting the normalization are extremely pertinent.

Any model for $\xi(W)$ also influences the normalization. Suppose that the phase shift passes rapidly through $\frac{1}{2}\pi$ at resonance and eventually reaches an asymptotic value $\xi(\infty)$ when $W' \gtrsim U$. Then we obtain

$$X(W) \simeq \exp\left[\frac{W-W_0}{\pi}\int_{W_0}^{U}\frac{\xi(W')dW'}{(W'-W_0)(W'-W-i\epsilon)} + \frac{W-W_0}{\pi}\xi(\infty)\int_{U}^{\infty}\frac{dW'}{(W'-W_0)(W'-W)}\right]$$

$$= \left(\frac{U-W_0}{U-W}\right)^{\xi(\infty)/\pi}\exp\left[\frac{W-W_0}{\pi}\int_{W_0}^{U}\frac{\xi(W')dW'}{(W'-W_0)(W'-W-i\epsilon)}\right]. \tag{D4}$$

Compared to the exponential, which varies rapidly over the region of the resonance, the factor in front is roughly constant in W. Thus we see that the asymptotic behavior of $\xi(W)$ has only slight influence on the resonance shape. The normalization, however, is quite strongly affected. Even for U as far past the resonance as $W_R + 2\Gamma$, the factor in front of the exponential is as large as 1.7 when $\xi(\infty) = \pi$ and $W = 1236$ MeV. If we were to truncate the integral at U, then this factor would not be present at all. The variation of the exponential with U is also measured by this factor, since the product is roughly independent of U.

With regard to the evaluation of $X(W)$, our approach is quite different from Adler's. He chooses a phenomenological phase shift, extrapolates it to large W, and performs the integration. The asymptotic region is handled in this fashion even though Adler claims to build his model from truncated dispersion integrals (Sec. 3C of Ref. 18). Adler thus uses the Omnès equation to produce an ansatz for his truncated fixed-momentum-transfer dispersion relations, and he supports this procedure by showing the equivalence of these equations in the static limit. Truncating one and not the other would break this equivalence. Furthermore, Eq. (D4) indicates that the exponential is sensitive to the value chosen for U.

Rather than build uncertain models for the asymptotic behavior of an eigenphase shift, we have ascertained the integral of $|X(W)|^2$ (which we call $\mathcal{I}$) by a comparison with electroproduction data. Numerically, our value for $\mathcal{I}$ is approximately four times as great as $\mathcal{I}_a$, where $\mathcal{I}_a$ is the corresponding value in Adler's calculation, given by

$$\mathcal{I}_a = \int |X(W)/X(m)|^2 dW \tag{D5}$$

using Adler's model for $X(W)$.

The calculations do agree, however, for low-k^2 electroproduction, since our A^{lhs} differs from Adler's A^B mainly because of our inclusion of ω^0 exchange. Both the magnitude and the k^2 dependence of A^{lhs} are affected, but for $k^2 \lesssim 0.5$ GeV^2 the change in k^2 dependence produced by adding the ω is slight. (At larger values of k^2, the electroproduction data do support our model in preference to Adler's.) Although it varies like the other contributions at small k^2, the ω^0 term is large and interferes with the others destructively. As a result, our values for A^{lhs} (vector) are about half the size of Adler's A^B (vector) when k^2 is small. Combined with our larger norm, this produces similar predictions for $N^*(1236)$ electroproduction.

As neither A^{lhs} nor $X(W)$ can be observed independently, we look for other processes that can further distinguish between the models. (Our experience with the higher resonances, for example, also supports inclusion of ω^0 exchange in A^{lhs}.) Since our model for weak production involves the new function A^{lhs} (axial) used with the same $X(W)$, we can gain indirect information about the enhancement factor by looking at the axial-vector contribution. In the axial-vector case, Adler's excitation function is quite similar to ours. As a result, our larger enhancement factor leads to a prediction of a larger axial-vector amplitude. Thus we explain how two similar models which agree for small-k^2 electroproduction give dissimilar predictions for weak production. So far the CERN data seem to support our prediction, as shown in Fig. 10.

Adler and we both include vector-meson exchange in the axial-vector excitation functions. Since the ρ meson has smaller coupling constants than the ω, this contribution does not affect the amplitude much. At extremely small k^2 near the

forward direction, however, the contribution of the ρ exchange is more important. Data in this region would be particularly valuable since PCAC could thereby be tested.

Although Eqs. (D1) and (D2) are rather similar, Adler supports his model in a fashion different from ours. Instead of writing partial-wave dispersion relations, Adler assumes fixed-momentum-transfer dispersion relations, which are in general not equivalent. Projecting out the spin-$\frac{3}{2}$ channel in the static limit, he obtains an Omnès equation whose solution he uses as an ansatz away from the static region. This Omnès equation is the same as the one we obtained in Sec. III without restricting ourselves to the static limit. Since both models are approximate solutions to the same Omnès equation, it is not surprising that they have similar forms.

Adler's method of finding an approximate solution also differs. While we make approximations based on the values of A^{lhs} in the resonance region, Adler approximates the singularities of A^{lhs} away from the physical region. After dividing out some kinematic factors, Adler writes the excitation function in terms of its singularities:

$$A^B(W, k^2) = \frac{1}{\pi}\int_L \frac{\alpha^B(W', k^2)dW'}{W' - W}, \tag{D6}$$

where the integral is over the left-hand cuts. The exact Omnès solution can then be transformed to give

$$A(W, k^2) = X(W)\left[\frac{1}{\pi}\int_L \frac{\alpha^B(W', k^2)dW'}{X(W')(W' - W)} + \lim_{W\to\infty}\frac{A(W)}{X(W)}\right] \tag{D7}$$

and Adler assumes that the limit of A/X is zero. The cut in A^B nearest to the physical region crosses the real axis near $W = m$. Adler approximates it by two poles:

$$\alpha^B(W, k^2) \simeq -\tfrac{1}{2}\pi C(k^2)[\delta(W - m + ia) + \delta(W - m - ia)], \tag{D8}$$

where $C(k^2)$ is a known function and $a(k^2)$ is small when k^2 is small. It is straightforward to check and see that this approximation reproduces the model for $A^B(W, k^2)$ reasonably well in the region of the resonance. The integral in (D7), however, involves a different weighting, and it is therefore a very strong assumption that this approximate α^B will work well in that equation. Inserting it results in Eq. (D1). As an illustration of some of the difficulties inherent in this approach, we consider the case when subtractions are performed in Eqs. (D6) and (D7). Then we would still have a rigorous solution to the Omnès equation. Equation (D8) would still give the same $A^B(W, k^2)$ when used in Eq. (D6), but it would yield a nonresonant result when combined with Eq. (D7).

In spite of the disadvantages of depending on the value of $A^B(W, k^2)$ away from the physical region, this approach does have the advantage that the W variation of A^B is accounted for at least crudely. Our approach, on the other hand, approximates this variation as being unimportant. At large k^2, it may be unreasonable to approximate the cut in A^B by two poles, but at small k^2 the cut is very short and this approximation is more realistic.

Although his approach is quite different, Adler's resulting approximate Omnès solution is quite similar to ours, except for the presence of $X(m)$. This factor is introduced by the approximation, since the exact solution in Eq. (D7) is unchanged if $X(W)$ is replaced by $X(W)/X(m)$. Since the approximation in Eq. (D8) implies that A^B is zero when $W = m$, Adler's final-state enhancement function emerges as being subtracted at m rather than at W_0, the place where we stated that A^{lhs} was zero. Thus the two approaches support each other as regards the isolation of the k^2 dependence but differ on the matter of normalizations.

APPENDIX E: LEFT-HAND SINGULARITIES

The contributions of the graphs in Fig. 5 are given by

$$\left(\frac{2\omega_q E_1 E_2 \Omega^3}{m^2}\right)^{1/2}\langle q p_2^{(\text{out})}|J_\mu(0) + J_{\mu 5}(0)|p_1\rangle^{\text{lhs}}$$

$$= \frac{4\pi W}{m}J_\mu = -g_{\pi N}\cos\theta_c \bar{u}(p_2)\Big\{\tau_\alpha\tau_+\gamma_5\frac{1}{i(p_1 + k)\cdot\gamma + m}(F_1^V\gamma_\mu - F_2^V\sigma_{\mu\nu}k_\nu + F_A\gamma_5\gamma_\mu + iF_P\gamma_5 k_\mu)$$

$$+\tau_+\tau_\alpha(F_1^V\gamma_\mu - F_2^V\sigma_{\mu\nu}k_\nu + F_A\gamma_5\gamma_\mu + iF_P k_\mu)\frac{1}{i(p_2 - k)\cdot\gamma + m}\gamma_5$$

$$+(\tau_\alpha\tau_+ - \tau_+\tau_\alpha)(-i\gamma_5)\left[\frac{F_\pi}{(k - q)^2 + \mu^2}(2q_\mu - k_\mu) + (F_\pi - F_1^V)\frac{k_\mu}{k^2}\right]$$

$$+(\tau_\alpha\tau_+ - \tau_+\tau_\alpha)\left(\frac{-G_5^F}{2g_{\pi N}}\right)(4m_\rho\mu/3)^{1/2}F_{\rho\pi A}\frac{1}{(k - q)^2 + m_\rho^2}$$

$$\times\left(\delta_{\mu\nu}-\frac{k_\mu k_\nu}{k^2+\mu^2}\right)[g_{1\rho NN}\gamma_\nu - g_{2\rho NN}\sigma_{\nu\lambda}(k-q)_\lambda]$$

$$+(\tau_\alpha\tau_+ + \tau_+\tau_\alpha)\frac{g_{\omega\pi\gamma}g_{\omega NN}}{g_{\pi N}}F_{\omega\pi\gamma}\frac{1}{(k-q)^2+m_\omega{}^2}$$

$$\times[2\gamma_5(\gamma_\mu P\cdot k - k\cdot\gamma P_\mu) - im\gamma_5(\gamma_\mu\gamma\cdot k - k\cdot\gamma\gamma_\mu)]$$

$$+(\tau_\alpha\tau_+ + \tau_+\tau_\alpha)\frac{(-iF_P k_\mu)}{2m}\Big\}u(p_1)\,. \tag{E1}$$

The form factors and coupling constants are described in Sec. IV.

In order to find $A^{\rm lhs}$, we need to perform a partial-wave projection. There are two approaches. One is to define invariant amplitudes and group the terms in Eq. (E1) accordingly. Then the partial-wave projection is performed on each of the invariants. This is the familiar procedure and is illustrated in Ref. 10. Although Eq. (E1) has an exactly conserved vector current and no kinematic singularities, introducing conserved invariants produces kinematic singularities which disappear only when the terms are combined to give the (observable) helicity amplitudes.

On the other hand, we may do the partial-wave projection on Eq. (E1) term by term. By inverting Eq. (2.18) we obtain

$$\langle\lambda_2|\,T^J+U^J\,|\lambda_1\lambda_k\rangle = (4k^*q)^{1/2}\frac{1}{2}\int_{-1}^{1}d\cos\theta_p\,\mathfrak{D}^J_{\lambda_1-\lambda_k,\lambda_2}(-\phi_p,-\theta_p,\phi_p)J_\mu e_\mu(\lambda_k)\,, \tag{E2}$$

with $e_\mu(\lambda_k)$ the unit vector described after Eq. (2.18). The helicity amplitudes are then obtained using the parity combinations given in Sec. II, and the angular integral is performed numerically.

We have developed routines based on both these approaches and have compared the results of the two computer programs as a check on our numerical predictions. The second method is particularly suited for handling more complicated final hadronic states.

---

*Research sponsored by the U. S. Atomic Energy Commission under Contract No. AT(45-1)-2230.

[1]Malcolm Derrick (private communication).

[2]Malcolm Derrick and Ivan Muzinich (private communications).

[3]Phys. Today 23 (No. 9), 18 (1970).

[4]Although some authors introduce a parameter to describe the nucleon elastic axial-vector form factor $F_A(k^2)$, we assume proportionality to the electric form factor, as suggested by recent data. Section IV contains a discussion of the elastic form factors, which are needed as input in this calculation.

[5]I. Budagov, D. C. Cundy, C. Franzinetti, W. B. Fretter, H. W. K. Hopkins, C. Manfredotti, G. Myatt, F. A. Nezrick, M. Nikolić, T. B. Novey, R. B. Palmer, J. B. M. Pattison, D. H. Perkins, C. A. Ramm, B. Roe, R. Stump, W. Venus, H. W. Wachsmuth, and H. Yoshiki, Phys. Letters 29B, 524 (1969).

[6]R. P. Feynman and M. Gell-Mann, Phys. Rev. 109, 193 (1958).

[7]Stephen L. Adler, Phys. Rev. 135, B963 (1964).

[8]Y. Nambu, Phys. Rev. Letters 4, 380 (1960); J. Bernstein, S. Fubini, M. Gell-Mann, and W. Thirring, Nuovo Cimento 17, 757 (1960); M. Gell-Mann and M. Lévy, *ibid.* 16, 705 (1960).

[9]For clear discussions of PCAC and the equivalence of the various formulations, see Stephen L. Adler and Roger F. Dashen, *Current Algebras* (Benjamin, New York, 1968), Chap. 1; and Jeremy Bernstein, *Elementary Particles and Their Currents* (W. H. Freeman, San Francisco, 1968), Chap. 11.

[10]J. D. Walecka and P. A. Zucker, Phys. Rev. 167, 1479 (1968).

[11]P. L. Pritchett, J. D. Walecka, and P. A. Zucker, Phys. Rev. 184, 1825 (1969).

[12]Paul A. Zucker, Ph.D. thesis, Stanford University, 1971 (unpublished).

[13]These data are summarized by L. Mo, in *High Energy Collisions*, edited by C. N. Yang, J. A. Cole, M. Good, R. Hwa, and J. Lee-Franzini (Gordon and Breach, New York, 1969), p. 127; M. Breidenbach, Ph.D. thesis, Massachusetts Institute of Technology, 1970 (unpublished).

[14]F. W. Brasse, J. Engler, E. Ganssauge, and M. Schweitzer, Nuovo Cimento 55A, 679 (1968).

[15]A. A. Cone, K. W. Chen, J. R. Dunning, Jr., G. Hartwig, Norman F. Ramsey, J. K. Walker, and Richard Wilson, Phys. Rev. 156, 1490 (1967); 163, 1854(E) (1967).

[16]H. L. Lynch, J. V. Allaby, and D. M. Ritson, Phys. Rev. 164, 1635 (1967).

[17]For a phenomenological treatment see S. Berman and M. Veltman, Nuovo Cimento 38, 993 (1965). For use of higher symmetries see, for example, C. H. Albright and L. S. Liu, Phys. Rev. Letters 14, 324 (1965); 14, 532(E) (1965); Phys. Rev. 140, B748 (1965); 140, B1611 (1965); and G. Altarelli, G. Preparata, and R. Gatto, Nuovo Cimento 37, 1817 (1965). Dynamical calculations in a vein similar to ours include P. Dennery, Phys. Rev. 127, 664 (1962); N. Dombey, ibid. 127, 653 (1962); and Ph. Salin, Nuovo Cimento 48A, 506 (1967). A phenomenological treatment for the $N^*(1520)$ is given

by A. Bottino and G. Ciochetti, Lett. Nuovo Cimento 2, 780 (1969).

[18]Stephen L. Adler, Ann. Phys. (N.Y.) 50, 189 (1968).

[19]G. F. Chew, F. E. Low, M. L. Goldberger, and Y. Nambu, Phys. Rev. 106, 1345 (1957).

[20]S. Fubini, Y. Nambu, and V. Wataghin, Phys. Rev. 111, 329 (1958).

[21]S. D. Drell and J. D. Walecka, Ann. Phys. (N.Y.) 28, 18 (1964).

[22]L. N. Hand, Phys. Rev. 129, 1834 (1963).

[23]R. Omnès, Nuovo Cimento 8, 316 (1958).

[24]N. I. Muskhelishvili, *Singular Integral Equations* (Noordhoff, Gröningen, 1953).

[25]We have chosen to subtract the equation at W_0 and have used the property that A and $A^{\rm lhs}$ are both zero at threshold. The mathematical solution follows by a procedure analogous to the ones discussed in the preceding references. A detailed discussion is also included in Ref. 12.

[26]Since $D(W)$ is given by an exponential, changes in the asymptotic behavior of ξ affect $D(W)$ quite sensitively. Although the normalization of $D(W)$ in the region of a resonance depends sensitively on the asymptotics, the variation of D with W does not. Appendix D contains a further discussion of this point.

[27]Since we make the approximation in Eq. (1.7) for each helicity, axial-vector and vector, our model requires the use of the same g for all of them. Thus the enhancement (due to the hadronic final-state interactions) of the axial-vector current is the same as for the vector current, which is the same as for electroproduction because of CVC.

[28]K. M. Watson, Phys. Rev. 88, 1163 (1952).

[29]The Omnès equation given in Eq. (1.5) expresses $A(W,k^2)$ in terms of its phase $\xi(W)$ above the physical cut and in terms of $A^{\rm lhs}$, the contributions coming from elsewhere. Unitarity then identifies $\xi(W)$ as the hadronic phase shift, implying the final-state theorem. Since $\xi(W)$ is the phase of A, it is always a real-valued function. Above the $\pi\pi N$ threshold the scattering phase shift is complex and the correspondence breaks down. In a hadronic eigenchannel, however, the eigenphase shift remains real, and unitarity identifies it with the phase of the eigenamplitude for all $W > W_0$. Thus in Eq. (1.6) $\xi(W)$ (which is rigorously the phase of A) can be taken as a scattering phase shift only for a hadronic eigenchannel.

[30]For discussions and observational results on the elastic nucleon form factors, see, for example, Robert Hofstadter, Rev. Mod. Phys. 28, 214 (1956); Ann. Rev. Nucl. Sci. 7, 231 (1957); R. Wilson, in *Proceedings of the International Symposium on Electron and Photon Interactions at High Energies, Hamburg, 1965,* (Springer, Berlin, Germany, 1965); G. Weber, in *Proceedings of the Third International Symposium on Electron and Photon Interactions at High Energies, Stanford Linear Accelerator Center, Stanford, California, 1967* (Clearing House of Federal Scientific and Technical Information, Washington, D. C., 1968), p. 59; R. E. Taylor, *ibid.*, p. 78.

[31]C. Franzinetti (private communication).

[32]This dependence is reviewed in Appendix B.

[33]For the use of coincidence experiments in electroproduction see P. L. Pritchett and P. A. Zucker, Phys. Rev. D 1, 175 (1970).

[34]We use a metric so that $a_\mu = (\vec{a}, ia_0)$. Our γ matrices are Hermitian and satisfy $\gamma_\mu\gamma_\nu + \gamma_\nu\gamma_\mu = 2\delta_{\mu\nu}$. The Dirac equation is $(i\not{p}+m)\,u(p) = 0$, and the baryon spinors are normalized to $\bar{u}u = 1$. We normalize the lepton spinors, however, to twice the lepton mass (zero for neutrinos, $2m_l$ for muons or electrons). We set $\hbar = c = 1$ and have $\alpha = e^2/4\pi = \frac{1}{137}$. In this metric $\gamma_5 = \gamma_1\gamma_2\gamma_3\gamma_4$.

[35]Our interest lies in the c.m.-frame components of J_μ, since the partial-wave expansion will be performed in that frame. From their definition in Fig. 2, it is clear that the unit vectors $\hat{e}_{k1,k2,k3}$ are unchanged by the Lorentz transformation along $\hat{k}$ from the c.m. frame to the laboratory frame.

[36]The coordinate system shown in Fig. 2 differs from that used by Adler in Ref. 18. Our angle θ_{kq} is the same as his polar angle ϕ, but our ϕ_{kq} differs by $\frac{1}{2}\pi$ from his azimuthal angle δ, with $\phi_{kq} = \delta + \frac{1}{2}\pi$.

[37]Equation (2.15) gives the definition of J_C and J_D in the c.m. frame. We shall define "C" and "D" combinations similarly for any frame using the components of k_μ in the frame under consideration.

[38]M. Jacob and G. C. Wick, Ann. Phys. (N.Y.) 7, 404 (1959).

[39]We use the angular momentum notation of A. R. Edmonds, *Angular Momentum in Quantum Mechanics* (Princeton Univ. Press, Princeton, N. J., 1957).

[40]In order to distinguish between these two longitudinal contributions, we shall attach an additional label to the initial states and to e_μ. Since all "helicity"-zero components behave the same way under the partial-wave expansion, it is often not necessary to distinguish J_C, J_D, J_0, J_3, or any other linear combination, and then this label will be suppressed.

[41]The helicity amplitudes $T^{J\pi}$ and $U^{J\pi}$ defined here are identical to those used in Refs. 12 and 33, although the $|\frac{3}{2}^{\pm}\rangle$ states were defined differently in those previous works. Walecka and Zucker (Ref. 10) used "parity amplitudes" $T^{J\pi}$ (with one helicity subscript) for electroproduction related to the present helicity amplitudes (when also defined for the electromagnetic current) by

$$T^{l\pm}_{3/2} = \mp\,(4k^*q)^{-1/2}\,T^{l\pm}_{1/2,\,3/2},$$

$$T^{l\pm}_{1/2} = (4k^*q)^{-1/2}\,T^{l\pm}_{1/2,\,1/2},$$

$$k^*L^{l\pm}/k_0 = (4k^*q)^{-1/2}\,T^{l\pm}_{1/2,\,C}.$$

By $l\pm$ we mean that $J = l \pm \frac{1}{2}$, and the parity is $(-1)^{l\pm1}$.

[42]If $\xi(W)$ goes to π asymptotically, there is the possibility of an arbitrary constant at infinity, related to the limit of $A(W,k^2)/WX(W)$. An additional subtraction would remove this ambiguity at the cost of introducing a subtraction constant. If, on the other hand, ξ goes to a limit less than π, no such constant at infinity is possible. In contrast, it is always possible to add poles (in subtracted form) and still have a solution to the Omnès equation. Mathematically, such poles may be considered part of $A^{\rm lhs}$. Physically, we have put the direct-channel nucleon pole into $A^{\rm lhs}$ and have assumed that there are no other poles for positive W.

[43]More generally, it is possible to subtract the integral in $X(W)$ at a different point than the integral in the solution for $A(W,k^2)$ given in Eq. (3.6). In such a case Eq. (3.7) would have $A^{\rm lhs}(W,k^2)/X(W_0)$ as the first term in

the bracket.

[44]In Ref. 11 a model for $\xi(W)$ which used the observed pion-nucleon scattering phase shifts suggested that $\frac{1}{2}\pi$ is a plausible asymptotic limit for each resonant eigenphase.

[45]Even though $X(W)$ is thus approximated to be a symmetric Breit-Wigner shape, the threshold dependence present in $A^{\rm lhs}(W,k^2)$ implies an asymmetric shape for $A \simeq A^{\rm lhs}/D$. In Ref. 13 there are discussions of how the threshold behavior was parametrized in the data analysis.

[46]Philip L. Pritchett, Ph.D. thesis, Stanford University, 1970 (unpublished).

[47]If we did not subtract the Omnès equation, we could not accomodate the possibility that $\sin\xi$ may not go to zero asymptotically unless we assumed that A and $A^{\rm lhs}$ went to zero.

[48]Contrastingly, in an unsubtracted calculation, the region where $\xi(W)$ decreases from near π to an asymptotic limit of zero must always give an important contribution. If, on the other hand, π is taken as the asymptotic limit, then there is an undetermined constant at infinity in the Omnès solution.

[49]In the spin-$\frac{1}{2}$ partial wave there is a nucleon pole at $W=m$. For the higher-spin partial waves, there is a cut crossing the ReW axis near $W=m$. Except when $k^2 \approx 0$, this cut is very long and most of it is far from the physical region. Furthermore, the partial-wave projection introduces kinematic factors that vary. Clearly, this approximation should be scrutinized whenever the predictions of such a model are compared with data.

[50]In order for the subtracted Omnès equation and the solution in Eq. (3.7) to converge, we need

$$\lim_{W\to\infty} W^{[\xi(\infty)/\pi]-1}\,|A(W,k^2)| = 0$$

and similarly for $A^{\rm lhs}$.

[51]The electroproduction points were provided by Martin Breidenbach, who separated the resonant parts from the observed cross section (see also Ref. 13).

[52]S. D. Ecklund and R. L. Walker, Phys. Rev. 159, 1195 (1967); R. L. Walker, *ibid.* 182, 1729 (1969). These works contain a thorough partial-wave analysis of the photoproduction data.

[53]P. L. Pritchett, N. S. Thornber, J. D. Walecka, and P. A. Zucker, Phys. Letters 27B, 168 (1968). Here, several different approaches to electroproduction are compared and the model-dependent features are identified.

[54]M. Breidenbach (private communication).

[55]In Ref. 11 it is shown that the transformation coefficients for a two-channel model (obtained from the pion-nucleon phase shifts plus an assumption about the second eigenphase shift) do indeed vary slowly across a resonance. They may, however, have singularities below threshold which affect the approximation in Eq. (3.9).

[56]In Appendix D of Ref. 12, the Omnès equation is solved with this cut appearing explicitly. The contribution from this cut is then shown to be slowly varying for W near W_R.

[57]It is possible to interpret such nonpole contributions as coming from some of the off-shell parts of the vertices occurring in the particle-exchange diagrams.

[58]N. Cabibbo, Phys. Rev. Letters 10, 531 (1963).

[59]G. Segrè and J. D. Walecka, Ann. Phys. (N.Y.) 40, 337 (1966).

[60]A discussion of coincidence experiments and what can be learned from them is given in Ref. 33.

[61]Strictly speaking, such a relation pertains to each separate helicity eigenamplitude. Since the cross section is a nonlinear combination of different helicity amplitudes, this relation does not apply directly. Nevertheless, it serves as a good illustration for the discussion.

[62]C. J. Christensen, A. Nielsen, A. Bahnsen, W. K. Brown, and B. M. Rustad, Phys. Letters 26B, 11 (1967).

[63]M. L. Goldberger and S. B. Treiman, Phys. Rev. 110, 1178 (1958).

[64]E. J. Moniz (private communication).

[65]A possible problem is the resonance-background interference which we thereby neglect. Since we are dealing with a noncoincidence cross section, only background in the same partial wave can interfere. Furthermore, the peaks considered are high-spin levels which appear prominently in pion-nucleon scattering. In addition, the background amplitude is expected to have a small phase while the resonant amplitude passes through 90°, diminishing any interference.

[66]The electroproduction curves incorporate kinematic functions like the K's which cause more rapid variation at $\theta = 6°$ and small k^2 than is contained in $w_i/G_{Ep}{}^2$.

[67]Choosing ϵ_1, ϵ_2, and θ as independent variables rather than ϵ_1, W, and k^2 does not make the integration over the resonance any simpler. When θ is fixed and ϵ_2 varied across the resonance, k^2 also varies across the resonance. Since the w_i are very sensitive to k^2 when θ is small (as indicated in Table II), integrating over the resonance remains difficult.

[68]This procedure is entirely consistent since Breidenbach (Ref. 13) used threshold factors like those in Eq. (5.7) in isolating the resonant part of the experimental data.